Enhancing The Performace of Load Real Power Flow using Dual UPQC-Dual PV System based on Dual Fuzzy Sugeno Method

Amirullah[1*], Adiananda[1], Ontoseno Penangsang[2], and Adi Soeprijanto[2]

[1]Electrical Engineering Study Program, Faculty of Engineering, Universitas Bhayangkara Surabaya, Surabaya, Indonesia
[2]Department of Electrical Engineering, Faculty of Intelligent Electrical and Informatics Technology, Institut Teknologi Sepuluh Nopember, Surabaya, Indonesia
[1]amirullah@ubhara.ac.id[*], [1]adiananda@ubhara.ac.id, [2]ontosenop@ee.its.ac.id,
[2]Zenno_379@yahoo.com, [2]adisup@ee.its.ac.id
[*]Corresponding Author

Abstract: This paper proposes a dual UPQC system model supplied by two PV arrays and then called the 2UPQC-2PV system to enhance load real power flow performance in a 380 V (L-L) low-voltage 3P3W distribution system with a frequency of 50 Hz. The 2UPQC-2PV configuration is used to maintain the load voltage and enhance the real load power performance in the event of an interruption voltage disturbance on the source bus. The performance of the 2UPQC-2PV configuration is further validated with the 2UPQC and 2UPQC-1PV configurations. The simulation of disturbance in each model configuration consists of six operating modes (OMs) i.e. OM 1 (Sinusoidal-Swell-Non Linear Load or S-Swell-NLL), OM2 (S-Sag-NLL), OM 3 (S-Interruption-NLL or S-Inter-NLL), OM4 (Distorted-Swell-NLL or D-S-NLL), OM5 (D-Sag-NLL), and OM 6 (D-Inter-NLL). The Dual-Fuzzy-Sugeno (Dual-FS) control method is used to overcome the weaknesses of the dual-proportional-integral (Dual-PI) control in determining the optimum parameters of proportional and integral constants. In OM 3 and OM 6, the 2UPQC-2PV configuration with Dual-PI and Dual-FS controls is able to maintain a higher load voltage than the 2UPQC and 2UPQC-1PV configurations. In OM 6, the 2UPQC configuration with the dual PI and dual FS methods is able to produce the lowest average (Total Harmonic Distortion (THD) of load voltage compared to the 2UPQC-1PV and 2UPQC-2PV. In OM 3 and OM 6, the 2UPQC-2PV configuration with Dual-PI and Dual-FS controls is capable of producing higher real load power, compared to the 2UPQC and 2UPQC-1PV configurations. In OM 3 and OM 6, the 2UPQC-2PV configuration with the Dual-FS method is able to produce higher load real power, compared to the Dual-PI method. Furthermore, in OM 3 and OM 6, the 2UPQC-2PV configuration with the Dual-FS method is also able to produce higher dual-UPQC efficiency, compared to the Dual-PI method. In the case of interruption voltage disturbances with sinusoidal and distorted sources, the 2UPQC-2PV configuration with dual-FS control can enhance load real power performance and dual-UPQC efficiency better than dual-PI control.

Keywords: Load Real Power Flow, 2UPQC-2PV, Dual-FS, Dual-PI, THD

1. Introduction

In the last decades, the use of non-linear loads by customers has contributed to a decrease in power quality (PQ) in the power system, causing current distortion. On the other hand, the presence of sensitive loads and voltage distortion on the source bus also causes a number of voltage disturbances, thereby also causing a decrease in voltage quality. To solve the problem of worsening PQ due to the use of sensitive loads or non-linear loads on the load bus and voltage distortion on the source bus, a power electronics device is proposed, namely Unified Power Quality Conditioner (UPQC) [1]. The UPQC consists of a Series-Active Filter (AF) and a Shunt-AF connected in parallel via a DC-link capacitor and serves to overcome several of power quality problems on the source and load sides simultaneously [2]. The Series-Active Filter (AF) functions to reduce the several of disturbances on the source bus. Meanwhile, the Shunt-AF

Received: October 20th, 2020. Accepted: January 03rd, 2021
DOI: 10.15676/ijeei.2021.13.1.2

functions to reduce the current quality problems on the load bus [3]. The strategy of developing a three-phase shunt-AF to mitigate the power quality of the source flow has been carried out by several researchers. These methods are robust extended complex kalman filter (RECKF)-linear quadratic regulator (LQR) [4], modified dynamic distribution static compensator (DSTATCOM) [5], transformerless DSTATCOM [6], and modified instant power theory-fuzzy logic [7]. The reduced-rule fuzzy logic method to support the performance of series-AF or dynamic voltage restorer (DVR) in mitigating sensitive load voltages from various power quality problems i.e. distorted source voltage and sag/swell voltage has been observed in [8]. To unify the performance of the shunt-AF and the series-AF as well as to mitigate power quality problems on the source and load bus, the UPQC has been investigated. This equipment is a combination of a shunt-AF and a series-AF, as well as, both are connected in parallel via a common DC link circuit. The optimal method of parameters for weight factor extraction on trapezoidal membership function using fuzzy logic has been developed by [9] in a single UPQC circuit. To anticipate the failure of both inverters in a single UPQC circuit, a dual UPQC supply by PV was developed. The advantage is that it has a more reliable inverter circuit structure and control because if there is a disturbance in one of the inverters, this system is still able to operate normally This configuration uses a two-phase two-level inverter with a synchronous rotating reference frame to control voltage and current method [10]. The dual or interline UPQC consists of two active filters, namely Series-AF and Shunt-AF (parallel active filters), used to reduce harmonics and voltage/current imbalances. Different from the single UPQC, the dual UPQC has a Series-AF which is controlled as a sinusoidal current source, and a Shunt-AF which is controlled as a sinusoidal voltage source.

Implementation of dual UPQC circuit and control, to improve power quality on the source and load side of the low voltage distribution system has been done and discussed in several papers. The simplification technique UPQC control has been proposed in [11] and developed on the ABC reference frame using the sinusoidal reference synchronization theory. In [12], a comparison of two different controls has been carried out to generate the PWM reference signal using the α-β and d-q reference frames, respectively. The comparison of the operating performance of single UPQC and dual UPQC in a 3 phase 3 wire (3P3W) system under static disturbances, as well as dynamic disturbances, has been carried out through simulations [13] and experiments [14]. The simulation and experiment results verify that a dual UPQC is capable of producing better static and dynamic performance than a single UPQC. The improvement of power quality using dual UPQC under conditions of sudden load changes has been investigated [15]. The study, analysis, and implementation of the dual UPQC model can be connected to a 3P3W or three-phase four-wire (3P4W) [16] and 3P4W distribution system [17] with proportional-integral (PI) control have been applied to improve the power quality system. The analysis to balance reactive power between series-AF and shunt-AF on a dual UPQC using power angle control has been carried out by [18]. The simulation results show that the power angle control method is able to determine the load power angle between load and source voltage.

The experimental study of the PV-UPQC system connected to a single-stage 3P3W network with dual compensation strategies and feed-forward closed control (FFCL) has been carried out both in static and dynamic conditions, as well as different load and solar irradiance levels [19]. The UPQC-PV system control base on fractional open circuit algorithm control method [20], Space Vector Pulse Width Modulation (SVPWM) [21], and tests based on improved synchronous reference frame control on moving average filter [22] have been observed. The stability analysis and power flow through three-phase multi-function distributed generator (DG) series and parallel converters using a single-stage PV system connected to the UPQC using an islanded and connected mode on the 3P3W system have been simulated and validated through an experimental laboratory [23]. The weakness of [10],[18-23] is that the analysis is only performed on conditions of distorted voltage sources, sag/swell voltages, and unbalanced voltages as well as unbalanced currents and unbalanced currents due to non-linear loads. In [24], the UPQC-PV system is also proposed not only to mitigate sag voltage but also to maintain load voltage and supply load power from PV due to interruption voltage. However, the simulation

results show that the proposed system is still unable to overcome the drop in load voltage so that it is not fully able to meet the real power supply on the load side.

To overcome the malfunction of one of the inverters and the inability of the single UPQC-PV system to overcome the disturbance caused by the interruption voltage, several researchers proposed a Dual UPQC system supplied by PV arrays or hereinafter known as the dual UPQC-PV system. The use of multilevel inverters has also been simulated in a dual UPQC-PV system connected to a 3P4W system to mitigate sag voltages, load voltage harmonics, and source current harmonics under different solar irradiance [25]. In [26], the dual-UPQC system is supplied by two PV arrays using two separate DC-link circuits that were proposed from two three-phase voltage source converters (VSC). The weakness of system models in [25],[26] was that it only discussed one level of PV array integration and was used to mitigate voltage sag/swell, unbalance, and harmonics due to non-linear loads and was not implemented to overcome interruption to maintain load real power remains stable. Besides, the determination of the optimum proportional and integral gains as control parameters for the shunt active filter circuit in the dual UPQC-PV model was also a problem that must be found in a solution.

Referring to the above problems, the main contributions of this study are:

1. Designing a dual UPQC model supplied by two PV arrays and then called as the 2UPQC-2PV configuration on a 3P3W system to maintain load voltage, to enhance load real power performance, and efficiency of dual-UPQC circuits due to interruption voltage disturbances on the source bus. The dual UPQC circuit is located between the load bus and the source bus (PCC) which is then connected to the 3P3W grid via a 380 V (L-L) distribution line with a frequency of 50 Hz. Both of PV array 1 and PV array 2 consists of several PV panels with a maximum power PV of 600 W respectively.
2. Validation of the performance of the 2UPQC-2PV configuration with the 2UPQC and 2UPQC-1PV configurations to determine the best system configuration in maintaining the magnitude and THD of load voltage as well as enhancing the load real power performance and efficiency of the dual-UPQC in the condition of voltage interruption on the source bus.
3. Implementation of the dual-FS control method on the shunt-AF respectively i.e. 2UPQC-2PV, 2UPQC, and 2UPQC-1PV to overcome the shortage of PI control in determining proportional (K_p) dan integral (K_i) gains in the proposed model.
4. Validation of the results of the dual-FS with the dual PI control method on the shunt-AF circuit of the 2UPQC-2PV, 2UPQC, and 2UPQC-1PV to determine the best system control method in maintaining magnitude and THD of load voltage as well as enhancing load real power performance and efficiency of the dual-UPQC circuit in the condition of the voltage interruption at the source bus.

This paper is arranged as follows. Section 2 presents the proposed method, 2UPQC-2PV configuration system, simulation parameter, PV system, series-AF control, and shunt-AF control, PI and FS method, percentage of sag/swell, and interruption voltage, as well as the efficiency of 2UPQC-2PV, 2UPQC-1PV, and 2UPQC configurations. Section 3 presents results and discussion of load voltage, source current, THD of load voltage, THD of source current, source real power flow, load real power flow, series real power flow, shunt real power flow, PV1 power, and PV2 power using the FS validated with the PI method. The percentage of sag/swell and interruption voltage as well as the efficiency of the proposed dual-UPQC configuration using both FS and PI method are also analyzed. In this section, three configurations of dual-UPQC and six disturbance OMs are presented and the results are verified with Matlab-Simulink. Finally, this paper is concluded in Section 4.

2. Research Method

A. Proposed Method

This study aims to improve the load power flow performance with the dual UPQC system supplied by a PV array based on the dual-FS method on the 3P3W distribution system. Both of PV array 1 and PV array 2 consists of several PV panels with a maximum power PV of 600 W respectively. There are three power electronic devices proposed, i.e. Dual-UPQC (2UPQC),

Dual-UPQC-Single PV Array (2UPQC-1PV), and dual UPQC-dual PV array (2UPQC-2PV). The 2UPQC-2PV system is used to overcome the weaknesses of 2UPQC and 2UPQC-1PV system to maintain the magnitude of load voltage so that the load bus still gets a more stable active power supply in the event of a voltage interruption on the source bus. The dual UPQC circuit is located between the load buses and connected to the source bus (PCC) via a 380 V (L-L) low-voltage distribution line with a frequency of 50 Hz. The FS controller is proposed to overcome the weakness of the PI controller in the tuning of proportional (K_P) and integral gain (K_I) parameters. The proposed model of the 2UPQC-2PV system is presented in Figure 1. The disturbance on three dual UPQC systems is described in the following six OMs respectively below:

1. OM 1 (S-Swell-NLL), In OM 1, the system is connected to the NLL, and the sinusoidal source runs into a voltage of 50 % swell.
2. OM 2 (S-Sag-NLL): In OM 2, the system is connected to the NLL, and the sinusoidal source runs into a voltage of 50 % sag.
3. OM 3 (S-Inter-NLL): In OM 3, the system is connected to the NLL and the sinusoidal source runs into a voltage of 100% interruption.
4. OM 4 (D-Swell-NLL): In OM 4, the system is connected to the NLL, the source produces 5th and 7th odd-order harmonic components with the individual harmonic of 5 % and 2 %, respectively, and is subjected to a voltage swell 50%.
5. OM 5 (D-Sag-NLL): In OM 5, the system is connected to the NLL, the source produces 5th and 7th odd-order harmonic components with the individual harmonic of 5 % and 2 %, respectively, and is subjected to a voltage sag 50%.
6. OM 6 (D-Inter-NLL): In OM 6, the system is connected to the NLL, the source produces 5th and 7th odd-order harmonic components with the individual harmonic of 5 % and 2 %, respectively, and is subjected to a voltage interruption of 100%.

The total simulation time for all cases of disturbance is 0.7 sec with a duration of 0.3 sec between t = 0.2 sec to t = 0.5 sec.

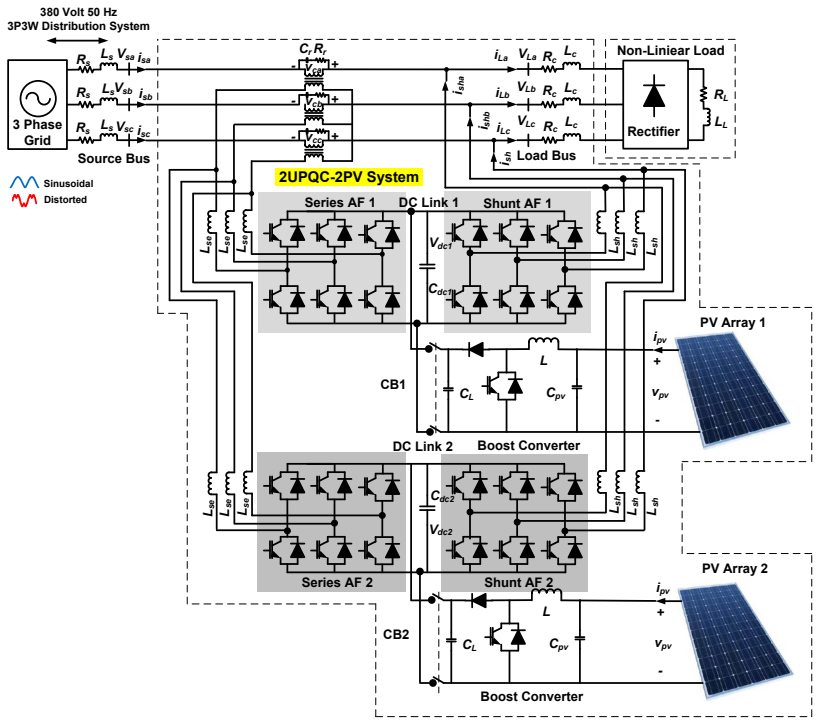

Figure 1. The proposed model of the 2UPQC-2PV system

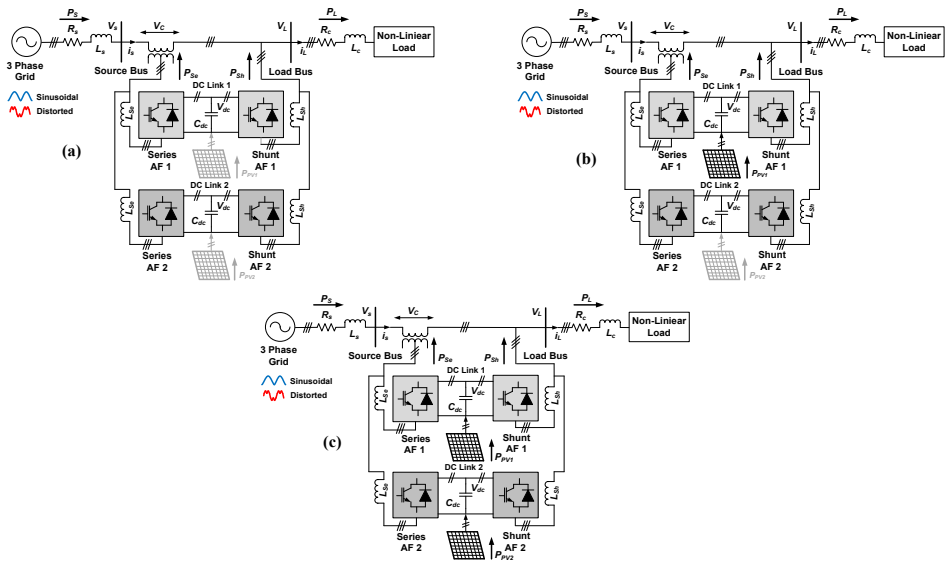

Figure 2. The real power flow of: (a) 2UPQC, (b) 2UPQC-1PV, (c) 2UPQC-2PV on a single-phase system

Table 1. Parameter of 2UPQC-2PV System

Devices	Parameters	Design Values
3P3W Grid	RMS Voltage (Line-Line) Frequency Line Impedance	380 Volt 50 Hz R_S = 0.1 ohm, L_S = 15 mH
Series-AF	Series Inductance	L_{Se} = 0.015 mH
Shunt-AF	Shunt Inductance	L_{Sh} = 15 mH
Series Transformer	Rating kVA Frequency Transformation Rating (N_1/N_2)	10 kVA 50 Hz 1 : 1
NNL	Resistance Inductance Load Impedance	R_L = 60 ohm L_L = 0.15 mH R_C = 0.4 ohm and L_C = 15 mH
DC Link 1 and 2	DC Voltage 1 and 2 Capacitance 1 and 2	V_{dc} = 650 volt C_{dc} = 3000 µF
Photovoltaic Array 1 and 2	Active Power Irradiance Temperature MPPT	0.6 kW 1000 W/m2 25^0 C Perturb and Observe
Proportional Integral (PI)1 and 2	Proportional Gain (K_P) 1 and 2 Integral Gain (K_I) 1 and 2	K_P=0.2 K_I=1.5
Fuzzy Logic Controller 1 and 2	Fuzzy Inference System Composition Defuzzyfication	Sugeno Max-Min wtaver
Input Memberships Function 1 and 2	Error V_{dc} ($V_{dc-error}$) Delta Error V_{dc} ($\Delta V_{dc-error}$)	trapmf and trimf trapmf and trimf
Output Membership Function 1 and 2	Instantaneous of Power Losses ($\bar{p}_{loss}$)	constant [0,1]

The FS control is implemented as a DC voltage control on the real shunt filter to enhance the power quality of each OM and the results are compared to the PI control. On each OM, each dual UPQC model uses PI and FS controls so a total of 12 OMs. The results analysis is carried out on parameters i.e. magnitude and THD of voltage and current on the source bus, magnitude and THD of voltage and current on the load bus, the source real power, the series real power, the shunt real power, the load real power, the PV1 power, and the PV2 power. After all these parameters have been obtained, the next step is to determine the percentage of load voltage disturbances and the efficiency of each dual-UPQC configuration as the basis for determining the circuit model that produces the best performance in maintaining the load voltage, the load current, and the load real power under six OM disturbances. Figure. 1 shows the proposed model using the 2UPQC-2P system. Figure. 2 shows the real power flow using a combination of 2UPQC, 2UPQC-1PV, and 2UPQC-PV in a single-phase system. The simulation parameters for the proposed model are shown in Table 1.

B. Photovoltaic Model

The equivalent circuit of the solar panel is shown in Figure. 3. It consists of several PV cells that have external connections in series, parallel, or series-parallel [27].

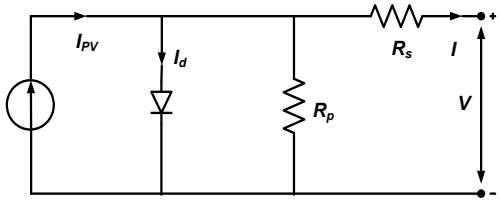

Figure 3. PV equivalent model

The V-I characteristic is presented in Equation (1):

$$I = I_{PV} - I_o \left[exp\left(\frac{V+R_S I}{a\, V_t}\right) - 1 \right] - \frac{V+R_S I}{R_P} \quad (1)$$

Where I_{PV} is PV current, I_o is saturated re-serve current, 'a' is the ideal diode constant, $Vt = N_S K T q^{-1}$ is the thermal voltage, N_S is the number of series cells, q is the electron charge, K is Boltzmann constant, T is temperature p-n junction, R_S and R_P are series and parallel resistance of solar panels. I_{PV} has a linear relationship with light intensity and also varies with temperature variations. I_o is a dependent value on the temperature variation. Equation (2) and (3) are the calculation of I_{PV} and I_o values:

$$I_{PV} = \left(I_{PV,n} + K_I \Delta T\right) \frac{G}{G_n} \quad (2)$$

$$I_o = \frac{I_{SC,n} + K_I \Delta T}{exp(V_{OC,n} + K_V \Delta T)/aV_t - 1} \quad (3)$$

Where $I_{PV,n}$, $I_{SC,n}$, and $V_{OC,n}$ are the PV current, short circuit current, and open-circuit voltage under environment conditions ($T_n = 25^0 C$ and $G_n = 1000\, W/m^2$), respectively. The K_I value is the coefficient of short circuit current to temperature, $\Delta T = T - T_n$ is temperature distortion from standard temperature, G is the irradiance level and K_V is the coefficient of open-circuit voltage ratio to temperature. By using (4) and (5) derived from the PV model equation, short-circuit current and open-circuit voltage can be calculated under different ambient environmental conditions.

$$I_{SC} = (I_{SC} + K_I \Delta T) \frac{G}{G_n} \quad (4)$$

$$V_{OC} = (V_{OC} + K_V \Delta T) \quad (5)$$

B. Control of Dual Series Active Filter

The Series-AF control on a single UPQC has been fully described in [24]. Based on this circuit model, the Series-AF control circuit on the dual UPQC is arranged by duplicating a single SeAF control circuit while still using one series of three-phase series transformers. Then based on this procedure, the authors further propose complete control of the dual UPQC whose model is shown in Figure. 4. The distorted source voltage is calculated and divided by the base input voltage peak amplitude V_m, as described in (6) [28].

$$V_m = \sqrt{\frac{2}{3}(V_{sa}^2 + V_{sb}^2 + V_{sc}^2)} \tag{6}$$

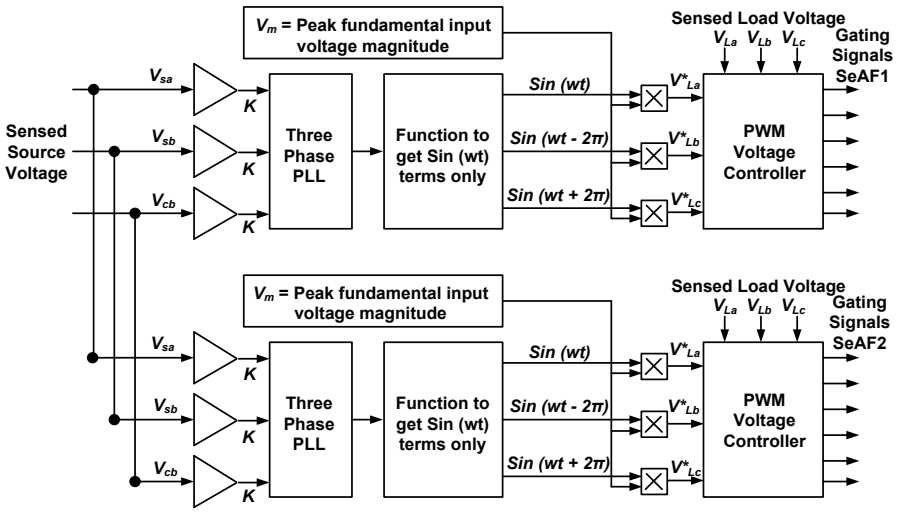

Figure 4. Control of dual series-AF

C. Control of Dual Shunt Active Filter based on Fuzzy Sugeno Method

The ShAF control on a single UPQC has been described in detail in [24]. Based on this circuit model, the dual UPQC ShAF control circuit is arranged by duplicating the control circuit on a single ShAF. Using the "p-q" method, the voltages and currents can be transformed into the $\alpha - \beta$. The axis is indicated in (7) and (8) [29].

$$\begin{bmatrix} v_\alpha \\ v_\beta \end{bmatrix} = \begin{bmatrix} 1 & -1/2 & -1/2 \\ 0 & \sqrt{3}/2 & -\sqrt{3}/2 \end{bmatrix} \begin{bmatrix} V_a \\ V_b \\ V_c \end{bmatrix} \tag{7}$$

$$\begin{bmatrix} i_\alpha \\ i_\beta \end{bmatrix} = \begin{bmatrix} 1 & -1/2 & -1/2 \\ 0 & \sqrt{3}/2 & -\sqrt{3}/2 \end{bmatrix} \begin{bmatrix} i_a \\ i_b \\ i_c \end{bmatrix} \tag{8}$$

The computation of real power (p) and imaginary power (q) is presented in (9) and (10) [28].

$$\begin{bmatrix} p \\ q \end{bmatrix} = \begin{bmatrix} v_\alpha & v_\beta \\ -v_\beta & v_\alpha \end{bmatrix} \begin{bmatrix} i_\alpha \\ i_\beta \end{bmatrix} \tag{9}$$

$$p = \bar{p} + \tilde{p} \;;\; q = \bar{q} + \tilde{q} \tag{10}$$

The total imaginary power (q) and fluctuating component of real power $(\tilde{p})$ are chosen as power and current references and are used by using (11) to balance the harmonics and reactive power [24].

$$\begin{bmatrix} i_{c\alpha}^* \\ i_{c\beta}^* \end{bmatrix} = \frac{1}{v_\alpha^2+v_\beta^2} \begin{bmatrix} v_\alpha & v_\beta \\ v_\beta & -v_\alpha \end{bmatrix} \begin{bmatrix} -\tilde{p} + \bar{p}_{loss} \\ -q \end{bmatrix} \quad (11)$$

The $\bar{p}_{loss}$ parameter is calculated from the voltage controller and is used as average real power. The compensation current ($i_{c\alpha}^*$, $i_{c\beta}^*$) is used to fulfill load power consumption as presented in (11). The current is stated in coordinates $\alpha - \beta$. The current compensation is needed to gain source current in each phase by using (7). The source current in each phase ($i_{sa}^*, i_{sa}^*, i_{sa}^*$) is stated in the ABC coordinates gained from the compensation current in $\alpha\beta$ axis and is expressed in (12) [30].

$$\begin{bmatrix} i_{sa}^* \\ i_{sb}^* \\ i_{sc}^* \end{bmatrix} = \sqrt{\frac{2}{3}} \begin{bmatrix} 1 & 0 \\ -1/2 & \sqrt{3}/2 \\ -1/2 & -\sqrt{3}/2 \end{bmatrix} \begin{bmatrix} i_{c\alpha}^* \\ i_{c\beta}^* \end{bmatrix} \quad (12)$$

In order to operate properly, the dual UPQC must have a minimum DC-link voltage(V_{dc}) stated in (13) [31]:

$$V_{dc} = \frac{2\sqrt{2}V_{LL}}{\sqrt{3}m} \quad (13)$$

The proposed system of a dual Shunt-AF control based on dual-FS method is presented by authors in Figure 5.

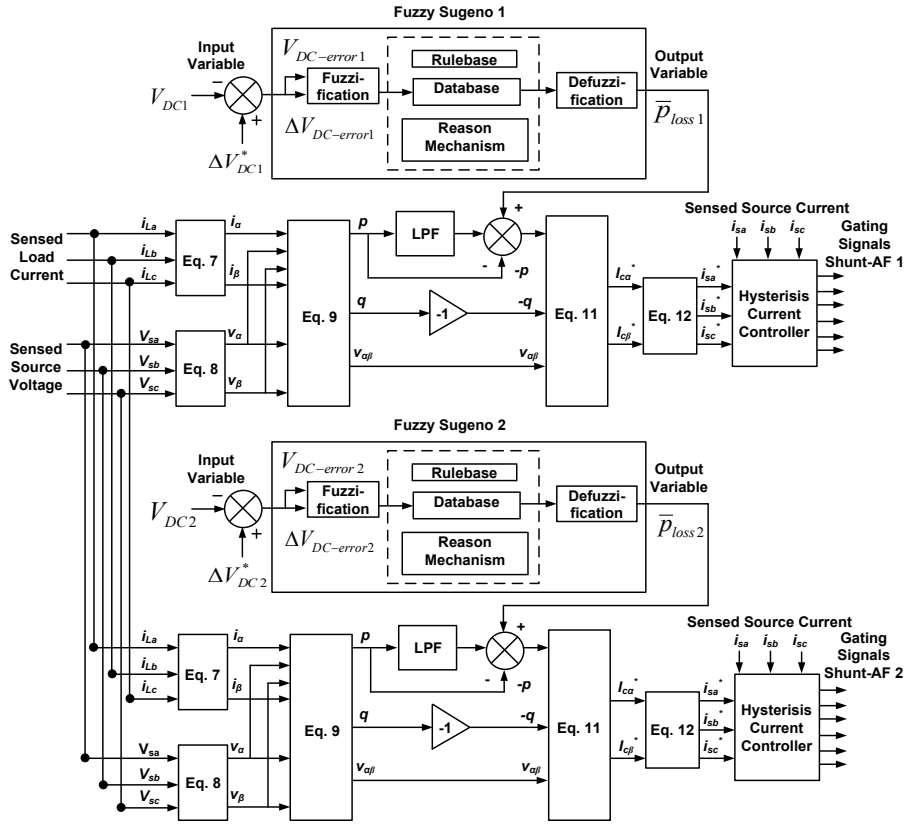

Figure 5. Control of dual shunt-AF based on dual FS model

Using the modulation value (m) equal to 1 and the line to line source voltage (V_{LL}) of 380 V, V_{dc} is calculated to be equal to 620.54 V and set at 650 V. The dual Shunt-AF input indicated in

Figure 5 is DC voltage 1 (V_{DC1}) and reference of DC voltage 1 (V_{DC1}^{*}) as well as DC voltage 2 (V_{DC2}) and reference of DC voltage 2 (V_{DC2}^{*}), while P_{loss1} and P_{loss2} are selected as the output of the FS 1 and FS 2 respectively. Furthermore, P_{loss1} and P_{loss2} will be input variable to generate the reference source currents ($i_{sa}^{*}, i_{sa}^{*}, i_{sa}^{*}$) in shunt-AF1 and shunt-AF2 Then, the reference source currents output is compared with the current sources (i_{sa}, i_{sb}, i_{sc}) by hysteresis current regulator to result in a trigger signal in the IGBT circuit of Shunt-AF 1 and Shunt-AF 2.

The FS is the development of Fuzzy-Mamdani (FM) in the fuzzy inference system represented in IF-THEN rules, where the output (consequent) of the system is not a fuzzy set, but rather a constant or linear equation. The FS method uses a singleton MF that has a membership degree of 1 at a single crisp value and 0 at another crisp value. The difference between FM and FS is the determination of the output crip resulting from the fuzzy input. The FM uses the defuzzification output technique, while FS uses a weighted average for computing the crips output. The ability to express and interpret the FM output is lost on the FS because the consequences of the rules are not fuzzy. Using this reason, then FS has a better processing time because it has a weighted average replacing the defuzzification phase which takes a relatively long time [32].

This research starts by determining $\bar{p}_{loss}$ as an input variable, to produce a reference source current on the hysteresis current control and to generate a trigger signal on the shunt active IGBT filter circuit from UPQC with PI1 and PI2 controls ($K_P = 0.2$ and ($K_I = 0.2$). Using the same procedure, $\bar{p}_{loss}$ is also determined using FS1 and FS2. The FS1 and FS2 sections comprise fuzzification, decision making (rulebase, database, reason mechanism), and defuzzification in Figure 5 respectively. The fuzzy inference system (FIS) in FS1 and FS2 uses Sugeno Method with a max-min for input and [0,1] for output variables. The FIS consists of three parts i.e. rulebase, database, and reason-mechanism [27]. The FS1 and FS 2 method is applied by determining input variables i.e. V_{DC} error ($V_{DC-error}$) and delta V_{DC} error ($\Delta V_{DC-error}$) value to determine $\bar{p}_{loss}$ in defuzzification phase respectively.

The value of $\bar{p}_{loss}$ is the input variables to obtain the compensation current ($i_{c\alpha}^{*}$, $i_{c\beta}^{*}$) in (24). During the fuzzification process, a number of input variables are calculated and converted into linguistic variables called the MFs. The $V_{DC-error}$ and $\Delta V_{DC-error}$ are proposed as input variables with $\bar{p}_{loss}$ output variables. In order to translate them, each input and output variable is designed using seven membership functions (MFs) i.e. Negative Big (NB), Negative Medium (NM), Negative Small (NS), Zero (Z), Positive Small (PS), Positive Medium (PM) and Positive Big (PB) shown in Table 2. The MFs of input and output crips are showed with triangular and trapezoidal MFs. The $V_{DC-error}$ ranges from -650 to 650, $\Delta V_{DC-error}$ from -650 to 650, and $\bar{p}_{loss}$ from -100 to 100 in FS 1 and FS 2 respectively. The input MF of $V_{DC-error}$, input MF of $\Delta V_{DC-error}$, and output MF of $\bar{p}_{loss}$ of FS 1 and FS 2 are presented in Figure. 6, Figure. 7, and Figure. 8 respectively.

After $V_{DC-error}$ and $\Delta V_{DC-error}$ are obtained, two input MFs are subsequently converted into linguistic variables and used as an input function for FS 1 and FS 2. Table 2 presents the output MF generated using the inference block and basic rules of FS 1 and FS 2. Then, the defuzzification block finally operates to change the $\bar{p}_{loss1}$ and $\bar{p}_{loss2}$ output generated from the linguistic variable to numeric again. The value of $\bar{p}_{loss1}$ and $\bar{p}_{loss2}$ then becomes the input variable for current hysteresis control to produce a trigger signal in the IGBT 1 and IGBT 1 of dual UPQC shunt active filter to reduce source current harmonics. Then at the same time, they also enhance PQ of 3P3W under six disturbance OMs of three configurations i.e. 2UPQC, 2UPQC-1PV, and 2UPQC-2PV respectively.

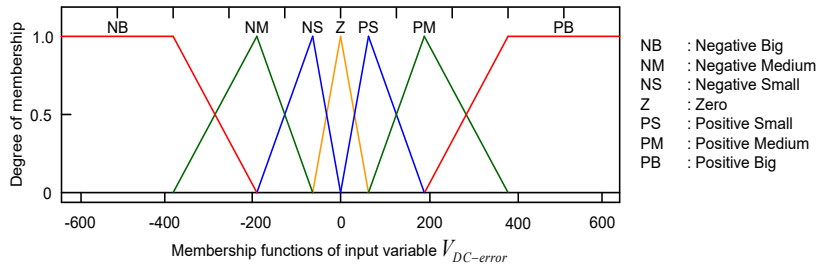

Figure 6. Input MFs of $V_{DC-error}$ for FS 1 and FS 2 respectively

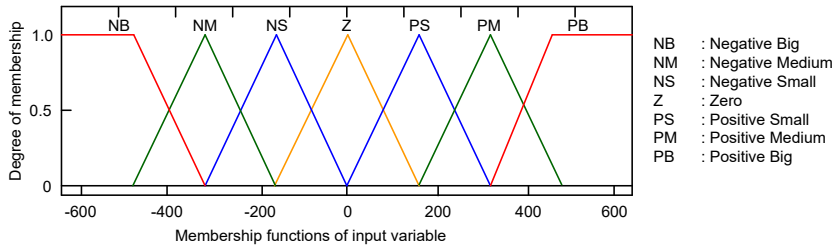

Figure 7. Input MFs of $\Delta V_{DC-error}$ for FS 1 and FS 2 respectively

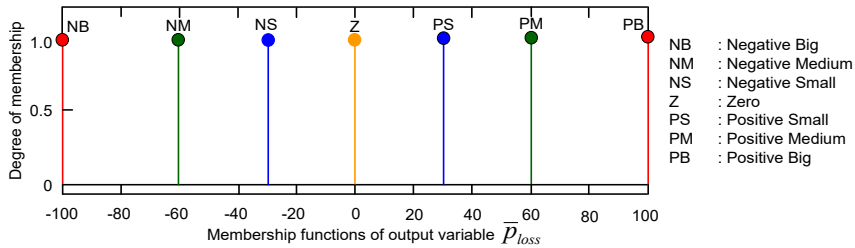

Figure 8. Output MFs of $\bar{p}_{loss}$ for FS 1 and FS 2 respectively

Table 2. Fuzzy Rule Base 1 and 2

$V_{DC-error}$ / $\Delta V_{DC-error}$	NB	NM	NS	Z	PS	PM	PB
PB	Z	PS	PS	PM	PM	PB	PB
PM	NS	Z	PS	PS	PM	PM	PB
PS	NS	NS	Z	PS	PS	PM	PM
Z	NM	NS	NS	Z	PS	PS	PM
NS	NM	NM	NS	NS	Z	PS	PS
NM	NB	NM	NM	NS	NS	Z	PS
NB	NB	NB	NM	NM	NS	NS	Z

D. Percentage of Sag/Swell and Interruption Voltage

The monitoring sag/swell and interruption are validated by IEEE 1159-1995 [33]. This regulation presents a table definition of voltage sag/voltage and interruption base on categories (instantaneous, momentary, and temporary) typical duration, and typical magnitude. The authors propose the percentage of disturbances i.e. sag/swell and interruption voltage in (14) below.

$$Disturb\ Voltage\ (\%) = \frac{|Vpre\_disturb - V\_disturb|}{Vpre\_disturb} \quad (14)$$

E. Efficiency of Dual UPQC Configuration

The investigation of 3-Phase 4-Leg Unified Series-Parallel Active Filter Systems using Ultra Capacitor Energy Storage (UCES) to mitigate sag and unbalance voltage has been presented in [34]. In this research, during the disturbance, UCES generates extra power flow to load through a series-AF via dc-link and a series-AF to load. Although providing an advantage of sag voltage compensation, the use of UCES in this proposed system is also capable of generating losses and efficiency systems. Using the same procedure, the authors propose (15) to determine the efficiency of 2UPQC-2PV, 2UPQC-1PV, and 2UPQC below.

$$E_{ff}\ (\%) = \frac{P_{Load}}{P_{Source} + P_{Series} + P_{Shunt} + P_{PV1} + P_{PV2}} \quad (15)$$

3. Results and Discussion

Table 3. Magnitude of Voltage and Current Using 2UPQC

OM	Source Voltage V_S (V)				Load Voltage V_L (V)				Source Current I_S (A)				Load Current I_L (A)			
	A	B	C	Av	A	B	C	Av	A	B	C	Av	A	B	C	Av
Dual-PI Method																
1	464.8	464.8	464.8	464.80	310.4	310.4	310.5	310.43	10.45	10.46	10.44	10.450	8.605	8.604	8.604	8.604
2	154.1	154.1	154.1	154.10	309.4	309.5	309.4	309.43	13.84	13.90	13.92	13.887	8.567	8.557	8.574	8.566
3	1.728	1.634	1.868	1.7433	256.5	245.0	268.1	256.53	16.61	15.42	19.94	17.323	7.323	6.800	7.192	7.105
4	464.8	464.8	464.8	464.80	318.9	321.9	325.9	322.23	10.97	10.86	10.92	10.917	8.916	8.934	8.934	8.928
5	154.3	154.3	154.2	154.27	297.3	299.0	295.6	297.30	12.12	12.68	12.68	12.493	8.286	8.342	8.098	8.242
6	1.404	1.473	1.621	1.4993	266.4	267.1	266.3	266.60	12.66	13.27	16.71	14.213	7.018	7.441	7.365	7.275
Dual-FS Method																
1	464.8	464.8	464.8	464.80	310.4	310.5	310.6	310.50	10.40	10.35	10.40	10.383	8.604	8.605	8.609	8.606
2	154.1	154.1	154.0	154.07	309.5	309.5	309.5	309.50	13.86	13.77	13.96	13.863	8.577	8.576	8.575	8.576

OM	Source Voltage V_s (V)				Load Voltage V_L (V)				Source Current I_S (A)				Load Current I_L (A)			
	A	B	C	Av	A	B	C	Av	A	B	C	Av	A	B	C	Av
3	2.164	1.897	2.948	2.3400	206.3	174.1	247.2	209.20	22.46	15.83	26.49	21.593	6.333	4.316	6.325	5.658
4	464.8	464.8	464.8	464.80	319.4	321.9	326.2	322.50	10.96	10.84	10.90	10.900	8.927	8.935	8.997	8.953
5	154.3	154.3	154.2	154.27	297.4	298.8	295.7	297.30	12.02	12.55	12.62	12.397	8.294	8.326	8.097	8.239
6	2.297	1.818	2.008	2.0400	260.70	203.5	159.9	208.03	22.29	18.54	17.11	19.313	7.140	6.668	4.643	6.150

Table 4. Magnitude of Voltage and Current Using 2UPQC-1PV

OM	Source Voltage V_s (V)				Load Voltage V_L (V)				Source Current I_S (A)				Load Current I_L (A)			
	A	B	C	Av	A	B	C	Av	A	B	C	Av	A	B	C	Av
Dual-PI Method																
1	464.8	464.8	464.8	464.80	310.0	310.0	309.9	309.97	10.45	10.46	10.47	10.460	8.590	8.578	8.584	8.584
2	154.2	154.2	154.2	154.20	309.5	309.6	309.5	309.53	13.16	13.18	13.18	13.173	8.578	8.578	8.578	8.578
3	1.911	1.917	2.002	1.9433	282.5	289.87	295.5	289.29	17.72	17.08	17.68	17.493	7.904	7.854	8.027	7.928
4	464.8	464.8	464.8	464.80	3200	322.9	326.9	323.27	11.12	11.03	11.03	11.060	8.956	8.946	9.000	8.967
5	154.3	154.3	154.3	154.30	297.6	297.6	297.6	297.60	11.83	12.44	12.37	12.213	8.277	8.364	8.116	8.252
6	1.692	2.566	1.934	2.0640	265.8	259.0	282.5	269.10	16.01	23.52	17.03	18.853	7.410	7.167	7.798	7.458
Dual FS Method																
1	464.8	464.8	464.8	464.80	309.9	310.1	310.1	310.03	10.34	10.33	10.32	10.330	8.584	8.587	8.591	8.587
2	154.2	154.2	154.2	154.20	309.9	309.6	309.6	309.70	12.97	12.96	13.02	12.983	8.577	8.579	8.579	8.578
3	2.471	2.184	1.553	2.070	208.3	229.1	126.5	187.97	21.68	23.09	13.58	19.450	4.561	7.072	4.109	5.247
4	464.8	464.8	464.8	464.80	319.8	323.7	327.0	323.50	10.94	10.81	10.95	10.900	8.931	8.981	9.003	8.972
5	154.4	154.4	154.3	154.37	297.94	299.6	295.6	297.71	11.40	11.90	11.94	11.747	8.274	8.378	8.109	8.254
6	1.294	2.035	1.834	1.7200	182.4	239.5	270.1	230.67	11.92	17.96	18.41	16.097	6.106	6.135	7.741	6.661

The proposed model is determined using three dual-UPQC combined models connected to a 3P3W (on-grid) system via a DC-link circuit. Three dual UPQC combinations proposed i.e. 2-UPQC, 2UPQC-1PV, and 2UPQC-2PV. Two single-phase CBs are used to connect and to disconnect PV arrays 1 and 2 to DC-link 1 and DC-link 2 respectively. The disturbance simulation in each dual-UPQC combination consists of six OMs i.e. OM 1 (S-Swell-NLL),

OM2 (S-Sag-NLL), OM 3 (S-Inter-NLL), OM4 (D-Swell-NLL), OM5 (D-Sag-NLL), and OM 6 (D-Inter-NLL). Each dual-UPQC and OM combination uses FS control validated by the PI control for a total of 12 OMs.

Table 5. Magnitude of Voltage and Current Using 2UPQC-2PV

OM	Source Voltage V_s (V)				Load Voltage V_L (V)				Source Current I_S (A)				Load Current I_L (A)			
	A	B	C	Av	A	B	C	Av	A	B	C	Av	A	B	C	Av
Dual-PI Method																
1	464.8	464.8	464.8	464.80	310.2	310.0	310.1	310.10	10.42	10.49	10.47	10.460	8.598	8.584	8.582	8.588
2	154.2	154.2	154.2	154.20	309.4	309.3	309.3	309.33	12.8	12.6	12.88	12.760	8.573	8.575	8.574	8.574
3	205.52	185.830	196.71	196.02	293.4	304.5	305.0	300.97	16.28	16.90	16.89	16.690	8.122	8.335	8.398	8.285
4	464.7	464.8	464.7	464.73	319.7	323.6	327.3	323.53	11.33	11.07	11.55	11.317	8.932	8.971	9.021	8.975
5	154.4	154.3	154.2	154.30	297.2	299.5	295.9	297.53	11.55	12.57	12.25	12.123	8.272	8.352	8.125	8.250
6	1.434	1.471	1.826	1.580	288.1	278.1	292.0	286.07	13.68	15.22	16.33	15.077	7.955	7.811	7.963	7.910
Dual-FS Method																
1	464.8	464.8	464.8	464.80	310.3	310.4	310.0	310.23	10.36	10.38	10.36	10.367	8.596	8.602	8.585	8.594
2	154.2	154.2	154.2	154.20	309.4	309.4	309.4	309.40	12.61	12.49	12.71	12.603	8.575	8.574	8.574	8.574
3	1.822	2.385	1.170	1.7900	176.2	256.2	175.5	202.63	15.74	23.16	14.34	17.747	4.510	7.213	5.741	5.821
4	464.8	464.8	464.8	464.80	319.7	324.1	327.3	323.70	11.12	10.89	11.13	11.047	8.920	9.000	9.016	8.979
5	154.4	154.3	154.3	154.33	297.4	299.5	295.6	297.50	11.41	12.05	11.95	11.803	8.277	8.361	8.111	8.250
6	0.9786	1.299	1.359	1.2100	210.9	211.6	281.6	234.70	9.926	10.91	13.51	11.449	6.892	5.281	7.581	6.585

By using Matlab Simulink, then each model combination is run according to the desired OM to obtain curves for source voltage($V_{Sa},\ V_{Sa},\ V_{Sa}$), load voltage ($V_{La},\ V_{Lb},\ V_{Lc}$), compensation voltage ($V_{Ca},\ V_{Cb},\ V_{Cc}$), source current ($I_{Sa},\ I_{Sb},\ I_{Sc}$), load current ($I_{La},\ I_{Lb},\ I_{Lc}$), and DC-link voltage (V_{dc}). Based on this curve, then the average value of the source voltage(V_S), load voltage(V_L), source current (I_S), and load current(I_L) is obtained based on the value of the voltage and current in each phase obtained previously. Furthermore, THD of V_S, THD of V_L, THD of I_S, and THD of I_L in each phase, and their average value are also determined based on the curves obtained previously. The next process is to determine the value of source active power (P_S), series active power (P_{Se}) , shunt active power(P_{Sh}), load active power(P_L), PV1 power(P_{PV1}), and PV2 power(P_{PV2}). The measurement of nominal voltage and current at source and load bus, as well as active power flow for each combination of dual-UPQC, were carried out in one cycle starting at t = 0.35 sec. The results

of the average value of the source voltage (V_S), load voltage (V_L), source current (I_S), and load current (I_L) of the three dual-UPQC configurations based on the PI and FS control methods are presented in Table 3, Table 4, and Table 5 respectively. Using the same procedure, then the average THD of V_S, average THD of V_L, average THD of I_S, and average THD of I_L with three dual UPQC combinations and two methods are presented in Table 6, Table 7, and Table 8, respectively.

Table 3 shows that in OM 1, OM 2, OM 4, and OM5, the 3P3W system using 2UPQC with the PI control method is still able to maintain an average load voltage (V_L) between 297.30 V to 322.23 V. However, at OM 3 and OM 6, the average load voltage decreased to 256.53 V and 266.60 V. In the same configuration and using the FS control method as well as OM 1, OM2, OM4, and OM 5, the average load voltage increased slightly between 297.30 V and 322.50 V. However, at OM 3 and OM 6, the average load voltage drops to 209.20 V and 208.03 V respectively. Table 3 also shows that the 3P3W system uses 2UPQC on OM 1, OM 2, OM 4, and OM 5, with PI control method is still able to maintain the average load current (I_L) between 8,242 A to 8,928 A. However, at OM 3 and OM 6, the average load current decreases to 7,105 A and 7,275 A respectively. In the same configuration and using the control method FS as well as OM 1, OM 2, OM 4, and OM 5, the average load current increased slightly between 8.239 A to 8.953 A. However, at OM 3 and OM 6, the average load currents drops to 5.658 A and 6.160 A respectively.

Table 4 shows that in OM 1, OM 2, OM 4, and OM5, the 3P3W system using 2UPQC-1PV with the PI control method is still able to maintain an average load voltage(V_L) between 297.60 V to 323.27 V. However, at OM 3 and 6, the average load voltage drops to 269.10 V and 289.29 V. In the same configuration and using the FS control method as well as OM 1, OM 2, OM 4, and OM 5, the average load voltage increases slightly between 297.71 V to 323.70 V. However, at OM 3 and OM 6, the average load voltage drops to 187.97 V and 230.67 V respectively. Table 4 also shows that the 3P3W system uses 2UPQC-1PV on OM 1, OM 2, OM 4, and OM5, with the PI control method is still able to maintain the average load current (I_L) between 8.252 A to 8.967 A. However, at OM 3 and 6, the average load current drops to 7.928 A and 7.468 A. In the same configuration and using the control methods FS as well as OM 1, OM 2, OM 4, and OM 5, the average load current increases slightly between 8. 254 A to 8,972 A. However, at OM 3 and OM 6, the average load current drop to 5.247 A and 6.661 A respectively.

Table 5 shows that in OM 1, OM 2, OM 4, and OM5, the 3P3W system using 2UPQC-2PV with the PI control method is still able to maintain an average load voltage(V_L) between 297.53 V to 323.53 V. However, at OM 3 and 6, the average load voltage drops to 300.97 V and 286.07 V respectively. In the same configuration and using the FS control method as well as OM 1, OM 2, OM 4, and OM 5, the average load voltage increases slightly between 297.50 V up to 323.70 V. However, at OM 3 and OM 6, the average load voltage drops to 202.63 V and 234.70 V respectively. Table 5 also shows that the 3P3W system uses 2UPQC-2PV on OM 1, OM 2, OM 4, and OM5, with the PI control method is still able to maintain the average load current (I_L) between 8.250 A to 8.975 A. However, at OM 3 and 6, the average load current drops to 8.285 A and 7.910 A respectively. In the same configuration and using the control methods FS as well as OM 1, OM2, OM 4, and OM 5, the average load current increases slightly between 8.250 A to 8.979 A. However, at OM 3 and OM 6, the average load current drops to 5.281 A and 6.585 A respectively.

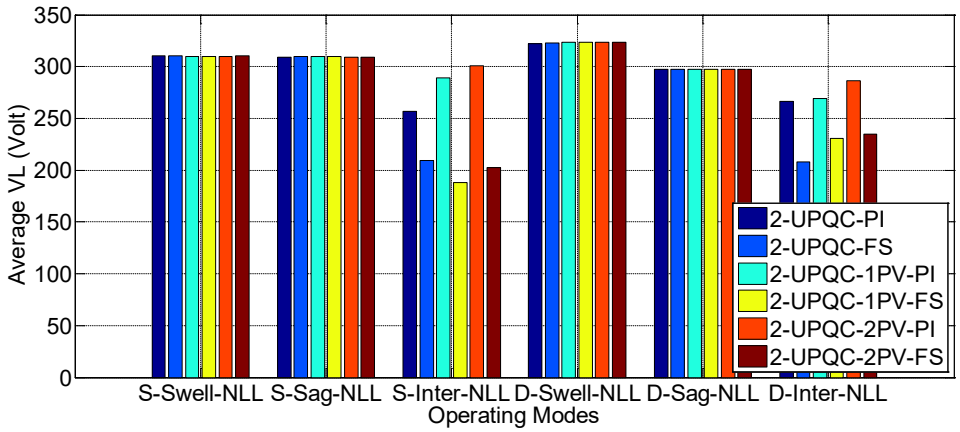

Figure 9. Performance of average load voltage under six OMs

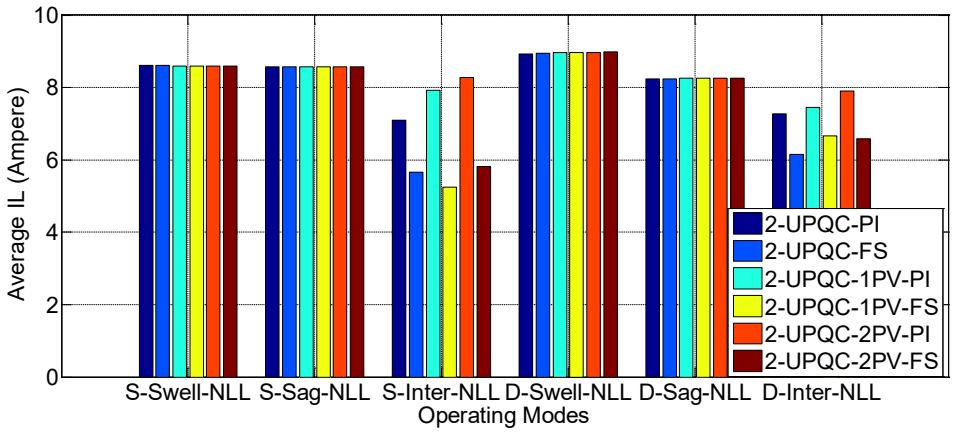

Figure 10. Performance of average load current under six OMs

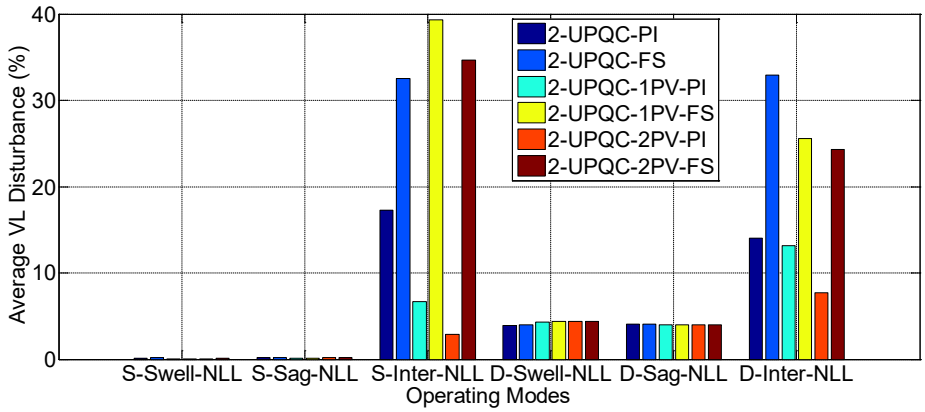

Figure 11. The performance of load voltage disturbance under six OMs

Figure. 9 and Figure. 10 present the performance of load voltage and load current respectively. Using Equation (14) and pre-disturbance voltage ($V_{pre\_disturb}$) as 310 V, the percentage of load average voltage on each OM and dual-UPQC configuration is obtained and the results are shown in Figure 11. They are a 3P3W system that using a configuration i.e. 2UPQC, 2UPQC-1PV, 2UPQC-2PV on six OM with dual PI, and dual FS methods.

Figure. 9 presents that the 3P3W system using three dual-UPQC configurations as well as dual PI and dual FS methods, the OM 4 is able to maintain a higher load voltage (V_L above 322.23 V) than the OM 1 (V_L above 309.97). This condition presents that the source voltage distortion in the Swell-NL disturbance causes an increase in load voltage compared to the source voltage without distortion. In the same three dual-UPQC configurations and using PI and FS methods, OM 4 is able to keep the load voltage lower (V_L above 297.30 V) than OM 2 (V_L above 309.33). This condition indicates that the source voltage distortion in the Sag-NL disturbance causes a voltage drop compared to the source voltage without distortion. In the three dual-UPQC configurations, the OM 3 is able to keep the load voltage lower (V_L above 187.97 V) than the OM 6 (V_L above 208.30). In OM 3, the 2UPQC-2PV configurations with dual PI and dual FS method is able to result in the highest load voltage (V_L) of 300.97 V and 202.63, respectively, compared to the 2UPQC and 2UPQC-1PV configurations. In OM 6, the 2UPQC-2PV configuration with PI and FS method is also able to result in the highest load voltage (V_L) of 286.07 V and 234.07, respectively, compared to the 2UPQC and 2UPQC-1PV configurations

Figure. 10 presents that in a 3P3W system using three dual-UPQC configurations as well as the dual PI and dual FS methods, OM 4 is able to maintain a higher load current (I_L above 8.928 A) than the OM 1 (I_L above 8.604 A). This condition presents that the source voltage distortion in the Swell-NL fault causes an increase in load current compared to the undistorted source voltage. In the same condition, the OM 5 is able to keep the load current lower (I_L above 8.239 A) than the OM 2 fault (I_L above 8.566 A). This condition indicates that the source voltage distortion in the Sag-NL fault causes a decrease in load current compared to the undistorted source voltage. In the three dual-UPQC configurations, the OM 3 is able to keep the load current lower (I_L above 5.427 A) than the OM 6 fault (I_L above 6.150 A). In the OM 3 fault, the 2UPQC-2PV configuration with PI and FS method is able to result in the highest load current of 8.285 A and 5.821 A, respectively, compared to the 2UPQC and 2UPQC-1PV configurations. In the OM 6, the 2UPQC-2PV configuration with dual PI and dual FS method is also able to result in the highest load current of 7.910 A and 6.585 A, respectively, compared to the 2UPQC and 2UPQC-1PV configurations.

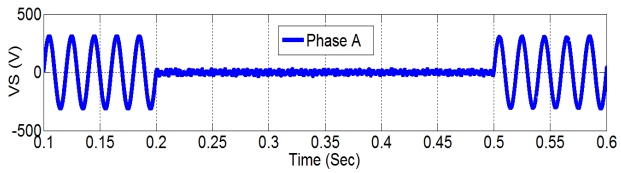

(a) 2UPQC

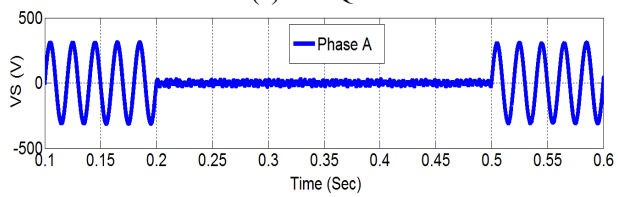

(b) 2UPQC-1PV

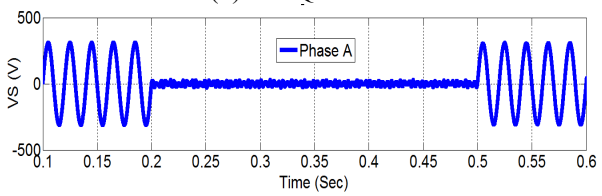

(c) 2UPQC-2PV

Figure 12. The performance of V_S on phase A using the FS method on OM 6 (D-Inter-NLL)

Figure 11 presents that in a 3P3W system using three dual-UPQC configurations and dual PI and dual FS methods, OM 4 is able to result a higher percentage of load voltage disturbances (V_D above 3.95% A) than OM 1 (V_D above 0.01%). This condition shows that the distortion of the source voltage in the Swell-NL fault causes an increase in the percentage of the voltage disturbance compared to undistorted source voltage. In the same conditions, OM 5 is able to result a higher percentage of voltage disturbances (V_D above 4 %) than OM 2 (V_D above 0.1%). This condition indicates that the distortion of the source voltage in the Sag-NL disturbances causes an increase in the percentage of the load voltage disturbances compared to the undistorted source voltage. In the three dual-UPQC configurations, OM 3 is able to produce a lower percentage of voltage disturbance (V_D above 2.91%) than OM 6 (V_D above 7.72%). In the OM 3, the 2UPQC-2PV configuration with dual PI and dual FS methods is able to result in the lowest percentage of voltage disturbances of 2.91% and 35.63%, respectively, compared to the 2UPQC and 2UPQC-1PV configurations. In the OM 6 fault, the 2UPQC-2PV configuration with PI and FS methods is also able to result in the lowest percentage of load voltage disturbance of 7.72% and 24.29%, respectively, compared to the 2UPQC and 2UPQC-1PV configurations.

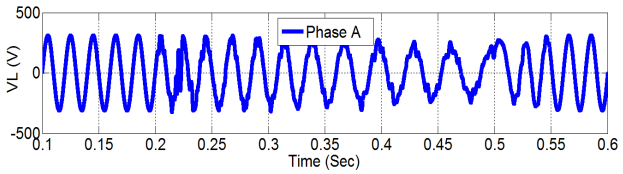

(a) 2UPQC

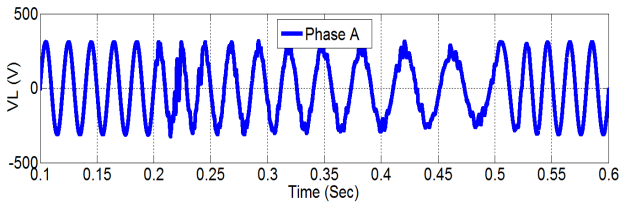

(b) 2UPQC-1PV

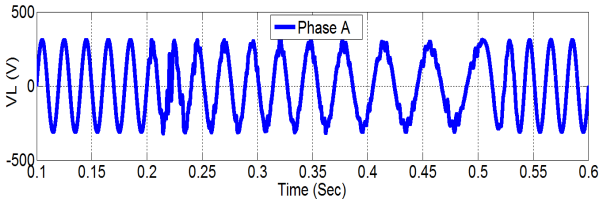

(c) 2UPQC-2PV

Figure 13. The performance of V_L on phase A using the FS method on OM 6 (D-Inter-NLL)

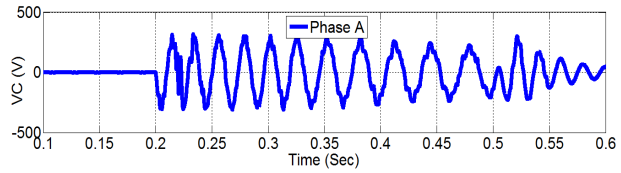

(a) 2UPQC

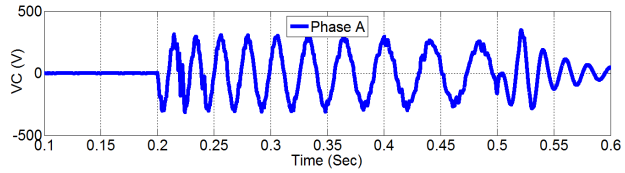

(b) 2UPQC-1PV

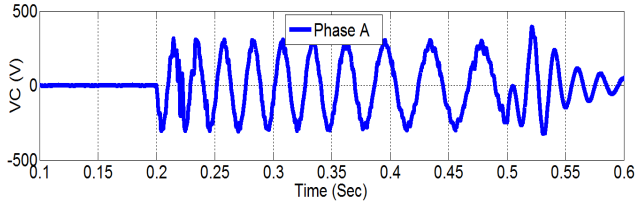

(c) 2UPQC-2PV

Figure 14. The performance of V_C on phase A using the FS method on OM 6 (D-Inter-NLL)

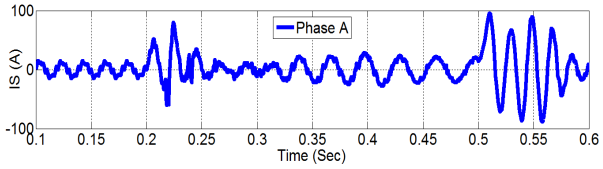

(a) 2UPQC

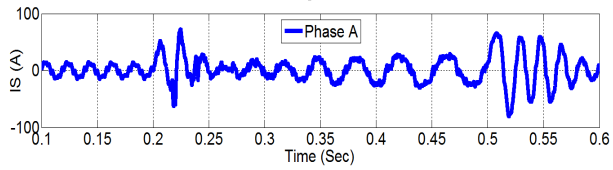

(b) 2UPQC-1PV

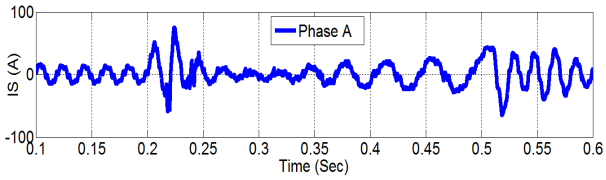

(c) 2UPQC-2PV

Figure 15. The performance of I_S on phase A using the FS method on OM 6 (D-Inter-NLL)

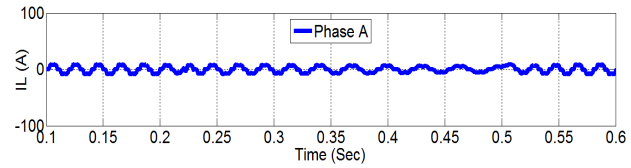

(a) 2UPQC

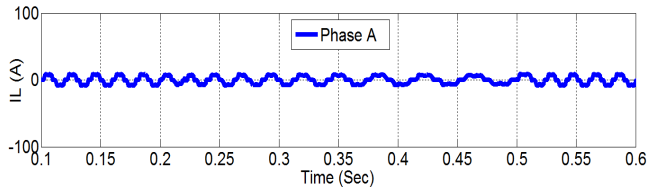

(b) 2UPQC-1PV

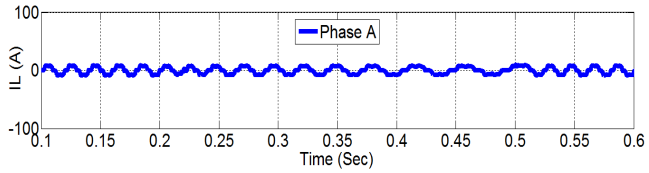

(c) 2UPQC-2PV

Figure 16. The performance of I_L on phase A using the FS method on OM 6 (D-Inter-NLL)

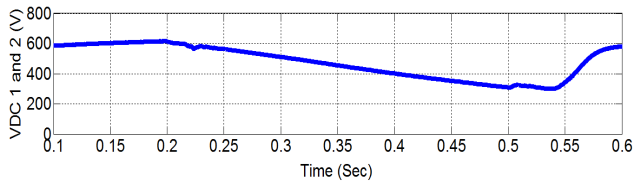

(a) 2UPQC

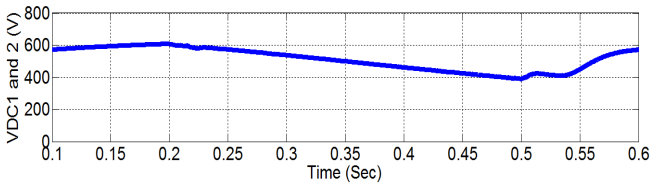

(b) 2UPQC-1PV

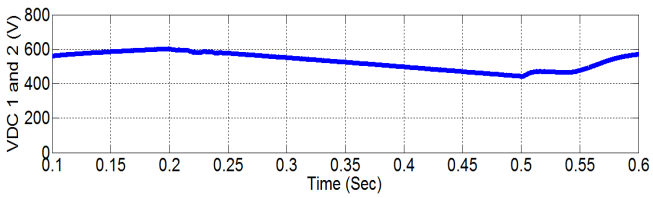

(c) 2UPQC-2PV

Figure 17. The performance of V_{DC1} and V_{DC2} using the FS method on OM 6 (D-Inter-NLL)

Figure. 12 to Figure. 17 presents the performance of the configuration of 2UPQC, 2UPQC-1PV, and 2UPQC-2PV respectively using the FS control method on OM 6 (D-Inter-NLL). Figure.12.a presents that in the 2UPQC configuration at t = 0.2 sec to t = 0.5 sec, the source voltage (V_S) on phase A drops 100% from 310 V to 2.297 V. Under these conditions, the DC-link capacitor C1 and C2 are not able to generate maximum power and are only able to inject the compensation voltage (V_C) on phase A of 258.403 (Figure. 14.a) through a series transformer

on a series active filter. So that in the OM 6 period, the load voltage (V_L) on phase A decreased by 260.70 V (Figure. 13.a). During the OM 6 fault, the DC-link capacitors C1 and C2 and the application of the FS method is not able to maintain DC 1 and DC 2 voltages (V_{DC1} and V_{DC2}) so that the value dropped significantly by 310 V (Figure. 17.a) as well as the load current (I_L) on phase A finally also decreases by 7.14 A (Figure. 16.a).

Figure. 12.b presents that in the 2UPQC-1PV configuration at t = 0.2 sec to t = 0.5 sec, the source voltage (V_S) on phase A drops 100% from 310 V to 1.294 V. Under these conditions, penetration of PV 1 array in DC-link 1 circuit is able to generate slightly maximum power and inject the compensation voltage (V_C) on phase A of 180.706 V (Figure. 14.b) through a series transformer on a series active filter. So that in the OM 6 period, the load voltage (V_L) on phase A increased slightly by 182.4 V (Figure. 13.b). During the OM 6 disturbance, the penetration of the PV 1 array and the application of the FS method is only able to slightly maintain the DC 1 and 2 DC voltages (V_{DC1} and V_{DC2}) so that their respective values decreased slightly to 390 V at t = 0.5 sec (Figure. 17.b) and causes it to be able to maintain the load current (I_L) on phase A remains constant at 6.106 A (Figure. 16.b).

Figure. 12.c presents that in the 2UPQC-2PV configuration at t = 0.2 sec to t = 0.5 sec, the source voltage (V_S) on phase A drops 100% from 310 V to 0.9786 V. The penetration of PV1 and PV2 arrays in DC-link 1 and 2 are able to generate maximum power and inject the compensation voltage (V_C) on phase A of 209.9214 V (Figure. 14.c) through a series transformer on a series active filter. So that in the OM 6 period, the load voltage (V_L) on phase A increases by 210.90 V (Figure. 13.c). During the OM 6 disturbance, the penetration of the PV 1 and PV 2 arrays and the application of the FS method are able to maintain both DC 1 and DC 2 voltages (V_{DC1} and V_{DC2}) so that the values decreased slightly to 440 V respectively at t = 0.5 sec (Figure. 17.c). Although the source current (I_S) on phase A drops to 9.926 A (Figure. 15.c) during the OM 6 period, the 2UPQC-2PV configuration is able to generate power and supply current through the shunt active filter so that I_L on phase A remains constant at 6,892 A (Figure. 16.c).

Table 6. Voltage and Current THD Using 2UPQC

OM	$THD\ V_S$ (%)				$THD\ V_L$ (%)				$THD\ I_S$ (%)				$THD\ I_L$ (%)			
	A	B	C	Av	A	B	C	Av	A	B	C	Av	A	B	C	Av
Dual-PI Method																
1	1.3500	1.3600	1.3600	1.3600	2.0600	2.080	2.0700	2.070	36.90	36.91	37.09	36.97	22.36	22.35	22.37	22.36
2	2.4700	2.4400	2.4900	2.4700	1.2400	1.220	1.2600	1.240	24.07	23.98	24.14	24.06	22.36	22.35	22.38	22.36
3	147.28	154.60	132.19	144.69	16.530	13.10	18.560	16.06	21.00	16.69	19.94	19.21	24.30	22.91	22.82	23.34
4	3.6800	3.8200	3.9800	3.8300	5.3600	6.550	8.1600	6.690	36.71	36.46	37.11	36.76	22.40	22.17	22.54	22.37
5	10.870	10.970	11.640	11.160	6.9200	7.120	8.8600	7.630	28.85	26.10	29.88	28.28	22.15	23.19	23.14	22.83
6	1211.59	1139.13	1053.34	1134.69	11.210	11.64	7.4500	10.10	24.82	21.50	16.71	21.01	22.07	22.65	22.13	22.28
Dual-FS Method																
1	1.3600	1.3500	1.3300	1.3500	2.0700	2.0400	2.030	2.050	37.01	37.50	37.47	37.33	22.4	22.39	22.37	22.39
2	2.4500	2.3900	2.4400	2.4300	1.2300	1.2000	1.230	1.220	24.17	24.38	23.69	24.08	22.37	22.38	22.38	22.38

OM	$THD\ V_S$ (%)				$THD\ V_L$ (%)				$THD\ I_S$ (%)				$THD\ I_L$ (%)			
	A	B	C	Av	A	B	C	Av	A	B	C	Av	A	B	C	Av
3	133.31	165.38	92.790	130.49	43.230	30.530	49.01	40.92	48.81	36.87	46.96	44.21	58.41	43.72	55.42	52.52
4	3.6900	3.8100	3.9700	3.8200	5.4200	6.4900	8.120	6.680	36.87	36.87	37.02	36.92	22.35	22.32	33.52	26.06
5	10.880	10.940	11.630	11.1500	7.0900	7.0900	8.810	7.660	29.6	26.78	30.46	28.95	22.21	23.34	23.01	22.85
6	741.06	914.66	847.89	834.54	44.340	32.240	30.10	35.56	42.88	34.84	39.45	39.06	44.66	44.75	38.84	42.75

Table 7. Voltage and Current THD Using 2UPQC-1PV

OM	$THD\ V_S$ (%)				$THD\ V_L$ (%)				$THD\ I_S$ (%)				$THD\ I_L$ (%)			
	A	B	C	Av	A	B	C	Av	A	B	C	Av	A	B	C	Av
Dual-PI Method																
1	1.1400	1.1100	1.1300	1.1300	1.7400	1.690	1.720	1.720	37.04	35.67	36.78	36.50	22.35	22.36	22.33	22.35
2	2.4300	2.3900	2.3800	2.4000	1.2300	1.190	1.190	1.200	26.25	26.16	26.55	26.32	22.37	22.36	22.37	22.37
3	175.84	175.42	193.21	181.49	8.320	5.920	5.240	6.490	18.4	18.54	15.89	17.61	22.18	23.07	22.55	22.60
4	3.6100	3.7300	3.8900	3.7400	5.500	6.310	8.080	6.630	35.96	35.97	36.50	36.14	22.27	22.21	22.55	22.34
5	10.830	10.980	11.670	11.160	6.650	7.170	8.760	7.530	30.28	27.14	31.49	29.64	22.14	22.95	23.04	22.71
6	964.55	685.58	915.98	855.37	17.41	16.82	10.16	14.80	25.96	27.25	34.06	29.09	28.58	30.69	19.70	26.32
Dual FS Method																
1	1.0800	1.0400	1.0200	1.0500	1.6400	1.580	1.550	1.590	37.09	37.09	37.18	37.12	22.36	22.32	22.33	22.34
2	2.3600	2.3800	2.3500	2.3600	1.1800	1.180	1.180	1.180	26.70	26.71	26.51	26.64	22.38	22.36	22.38	22.37
3	119.07	141.12	170.61	143.60	58.950	56.690	31.72	49.12	59.49	61.38	40.28	53.72	75.97	63.28	49.88	63.04
4	3.6000	3.7300	3.8900	3.7400	5.0900	6.6300	8.060	6.590	36.89	36.07	35.52	36.16	22.54	21.96	22.56	22.35
5	10.820	10.980	11.620	11.140	6.6400	7.2100	8.880	7.580	30.97	28.09	31.82	30.29	22.19	22.84	23.13	22.72
6	1332.45	849.60	887.04	1023.03	28.460	37.170	49.19	38.27	41.51	51.27	18.41	37.06	49.36	46.40	49.42	48.39

Table 8. Voltage and Current THD Using 2UPQC-2PV

OM	$THD\ V_S$ (%)				$THD\ V_L$ (%)				$THD\ I_S$ (%)				$THD\ I_L$ (%)			
	A	B	C	Av	A	B	C	Av	A	B	C	Av	A	B	C	Av
Dual-PI Method																
1	1.1000	1.1800	1.1100	1.1300	1.700	1.810	1.700	1.740	36.84	36.84	36.72	36.80	22.31	22.35	22.35	22.34
2	2.7600	2.6100	2.6300	2.6700	1.400	1.320	1.320	1.350	27.29	27.11	27.52	27.31	22.39	22.37	22.38	22.38
3	205.52	185.53	196.71	195.92	9.910	6.210	6.050	7.390	20.52	21.39	17.58	19.83	24.79	22.4	22.94	23.38
4	3.6100	3.7300	3.9000	3.7500	5.250	6.440	8.180	6.620	35.37	36.53	35.83	35.91	22.54	22.12	22.55	22.40
5	10.870	11.040	11.710	11.210	6.950	6.890	8.970	7.600	30.94	26.88	33.36	30.39	22.20	23.28	23.07	22.85
6	1164.15	1440.89	988.51	1197.85	8.311	9.070	8.570	8.650	38.17	36.23	28.13	34.18	23.44	24.17	23.08	23.56
Dual-FS Method																
1	1.0600	1.0900	1.1700	1.1100	1.610	1.660	1.790	1.690	36.8	37.12	36.3	36.74	22.33	22.29	22.37	22.33
2	2.6600	2.6100	2.5700	2.6100	1.350	1.320	1.300	1.320	28.01	27.67	27.42	27.70	22.39	22.37	22.38	22.38
3	159.77	123.18	231.81	171.59	46.34	61.20	48.730	52.09	44.84	59.94	68.99	57.92	47.63	63.83	75.99	62.48
4	3.6000	3.7100	3.8900	3.7300	5.040	6.550	8.450	6.680	36.36	36.57	35.55	36.16	22.63	21.97	22.63	22.41
5	10.870	10.990	11.690	11.180	6.810	7.070	8.860	7.580	30.89	28.58	32.69	30.72	22.14	23.17	23.12	22.81
6	1733.41	1312.42	1247.08	1430.97	35.82	30.95	50.46	39.08	57.00	47.51	54.67	53.06	50.93	40.63	53.5	48.35

Table 6 shows that the combination of 2UPQC with PI control which experienced disturbance with OM 1, OM 2, and OM 3 is able to produce an average THD of load voltage of 2.07%, 1.24%, and 16.0%, respectively. The disturbance of OM 4, OM 5, and OM 6 using the same configuration and control are able to increase the average THD value of the load voltage to 6.69%, 7.63%, and 10.10%, respectively. If using the dual FS control, the disturbance of OM 1, OM 2, and OM 3 produces an average THD of load voltage of 2.05%, 1.22%, and 40.92%, respectively. In the same control, the disturbance of OM4, OM5, and OM6 is able to increase the average THD of the load voltage to 6.68%, 7.76%, and 35.56%, respectively. At OM6, the average THD of the load voltage decreased significantly by 35.56% compared to the average THD of the source voltage of 834.34%. In the 2UPQC configuration that experienced disturbance with OM 1, OM 2, OM 4, and OM 5, the dual PI and dual FS controls are able to increase the average THD of the source current compared to the average THD of the load current. On the other hand, the OM 3 and OM 6 dual PI and dual FS controls are able to reduce the average THD of the source current compared to the THD of the load voltage.

Table 7 shows that the combination of 2UPQC-1PV with PI control which experienced disturbance with OM 1, OM 2, and OM 3 is able to produce an average THD of load voltage of 1.72%, 1.20%, and 6.49% respectively. While at the same control with disturbance OM 4, OM 5, and OM 6, this configuration is able to increase the average THD of load voltage to 6.63%, 7.53%, and 14.80% respectively. If using dual-FS control, the disturbance of OM 1, OM 2, and OM 3 is able to produce an average THD of load voltage of 1.59%, 1.18%, and 49.12%, respectively. In the same configuration and control, disturbance of OM 4, OM 5, and OM 6 are able to increase an average THD of load voltage to 6,590%, 7,580%, and 38.27%, respectively. At disturbance OM 6, an average THD of load voltage decreased significantly by 38.27% compared to an average THD of the source voltage of 1023.03%. In the 2UPQC-1PV configuration that experiences disturbance with OM 1, OM 2, OM 4, and OM 5, dual PI and dual FS controls are able to increase the average THD of the source current compared to the average THD of the load current. On the other hand, the OM 3 and OM 6 disturbances using dual PI and dual FS controls are able to reduce the average THD of the source current compared to an average THD of the load current.

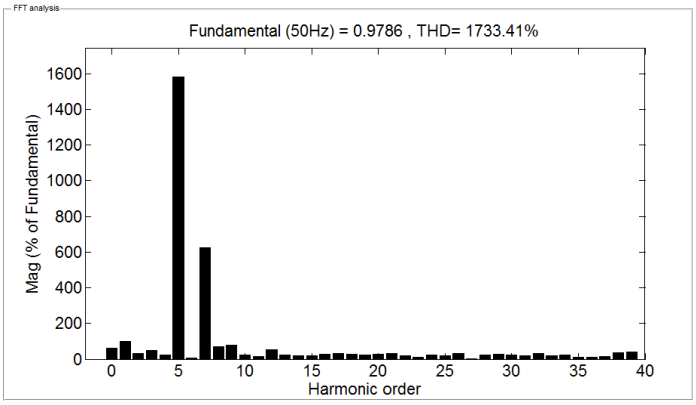

(a).

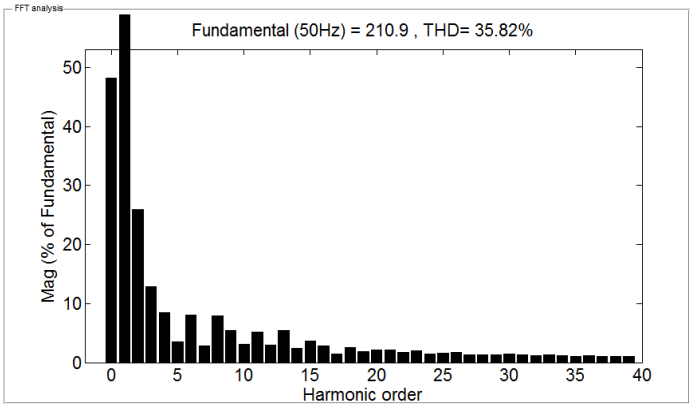

(b)

Figure 18. Harmonic spectra of: (a) V_S and (b) V_L on phase A for 2UPQC-2PV configuration using FS method

Table 8 shows that the combination of 2UPQC-2PV with dual-PI control which experienced disturbance OM 1, OM 2, and OM 3, is able to produce an average THD load voltage of 1,740%, 1.35%, and 7.39%, respectively. Whereas in the same control with disturbance OM 4, OM 5, and OM 6, this configuration is able to increase the average THD value of the load voltage to 6.62%, 7.6%, and 8.65%, respectively. If using dual-FS control, the disturbance OM1, OM2, and

OM 3 are able to produce an average THD of load voltages of 1,690%, 1.32%, and 52.09%, respectively. In the same configuration and control, the OM4, OM5, and OM6 disturbances are able to increase an average THD of the load voltage of 6,680%, 7,580%, and 39.08%, respectively. At the disturbance OM 6, an average THD of the load voltage decreased significantly by 39.08% compared to an average THD of the source voltage of 1430.07%. In the 2UPQC-2PV configuration which experienced disturbance OM 1, OM 2, OM 4, and OM 5, the dual PI and dual FS controls are able to increase the average THD of the source current compared to an average THD of the load current. On the other hand, the OM 3 and OM 6 using dual PI and dual FS controls are able to reduce the average THD of the source current compared to an average THD of the load current.

Figure 18 shows that in the OM 6 disturbance, the 2UPQC-2PV configuration using the dual FS method is able to produce THD of phase A load voltage of 35.82% significantly lower than THD of phase A source voltage of 1733.41%.

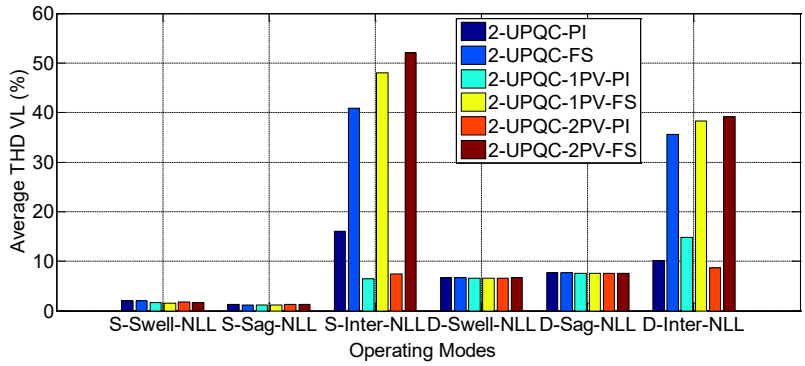

Figure 19. Performance of average harmonics of load voltage under six OMs

Table 9. Real power flow and efficiency of 2UPQC using PI and FS methods

OM	Source Power(W)	Series Power (W)	Shunt Power (W)	PV1 Power (W)	PV2 Power (W)	Load Power (W)	Eff (%)
PI method							
1	6060	-1960	-280	-	-	3728	97.592
2	2920	3000	-2100	-	-	3700	96.859
3	0	6400	-3500	-	-	2880	99.310
4	6300	-1900	-200	-	-	4030	95.952
5	2550	2430	-1400	-	-	3425	95.670
6	0	5400	-2150	-	-	2800	86.154
FS method							
1	6000	-1930	-225	-	-	3728	96.957
2	2870	2970	-2010	-	-	3700	96.606
3	0	9950	-7000	-	-	2660	90.169
4	6250	-1850	-250	-	-	4030	97.108
5	2500	2370	-1300	-	-	3425	95.938
6	0	9000	-6000	-	-	2900	96.667

Table 9, Table 10, and Table 11 present real power flow and efficiency for the configuration of (i) 2UPQC, (ii) 2UPQC-1PV, and (iii) 2UPQC-2PV using PI and FS methods.

Figure 19 shows that the 3P3W system uses three dual-UPQC configurations as well as the dual PI and dual FS methods, OM 4 is able to increase the average THD of a higher load voltage ($THD\ V_L$ above 6.59%) than OM 1 ($THD\ V_L$ above 1.59%). In three dual UPQC configurations using the PI and FS methods, OM 5 is also able to produce a higher average THD load voltage

($THD\ V_L$ above 7.53%) than OM 2 ($THD\ V_L$ above 1.18%). This condition shows that the source voltage with distortion in the Swell-NLL and Sag-NLL disturbances causes an increase in the average THD of the load voltage compared to the source voltage without distortion. In three dual UPQC configurations, OM 6 is able to produce the THD average load voltage is lower than OM 3. In OM 6, the 2UPQC configuration with the dual PI and dual FS methods is able to produce the lowest average THD load voltage ($THD\ V_L$) of 10.10% and 35.56% respectively compared to the 2UPQC-1PV and 2UPQC-2PV configurations.

Table 10. Real power flow and efficiency of 2UPQC-1PV using PI and FS methods

OM	Source Power(W)	Series Power (W)	Shunt Power (W)	PV1 Power (W)	PV2 Power (W)	Load Power (W)	Eff (%)
PI Method							
1	6100	-1900	-200	-250	-	3720	99.200
2	2730	2880	-1700	550	-	3703	83.027
3	0	6650	-3100	1200	-	3400	71.579
4	6500	-1800	-250	-200	-	4200	98.824
5	2500	2500	-1300	530	-	3430	81.087
6	0	6250	-2800	950	-	2900	65.909
FS Method							
1	6100	-1800	-235	-290	-	3712	98.331
2	2690	2780	-1647	556	-	3700	84.494
3	0	11800	-8370	1150	-	3200	69.869
4	6500	-1750	-350	-300	-	4060	99.024
5	2400	2270	-1050	560	-	3430	82.057
6	0	8000	-5000	1100	-	3150	76.829

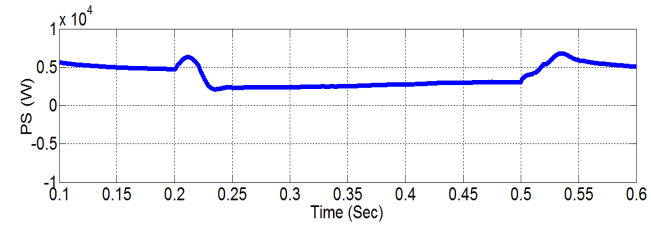

(a) 2UPQC

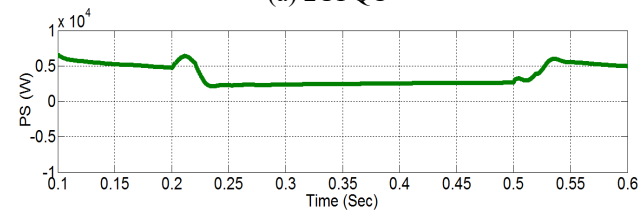

(b) 2UPQC-1PV

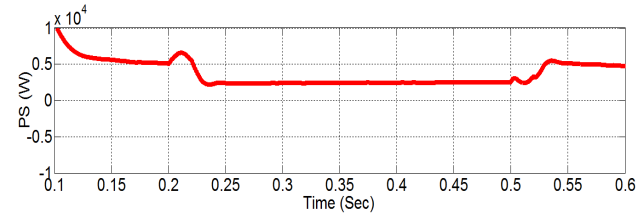

(c) 2UPQC-2PV

Figure 20. The performance of P_S using the FS method on OM 5 (D-Sag-NLL)

Figure 20 to Figure. 24 present the performance of: P_S, P_{Se}, P_{Sh}, P_L, and P_{PV} for the configuration of: (a) 2UPQC, (b) 2UPQC-1PV, and (c) 2UPQC-2PV respectively, using the FS method on OM 5 (D-Sag-NLL).

Table 11. Real power flow and efficiency of 2UPQC-2PV using PI and FS methods

OM	Source Power(W)	Series Power (W)	Shunt Power (W)	PV1 Power (W)	PV2 Power (W)	Load Power (W)	Eff (%)
PI Method							
1	6200	-1900	0	-250	-250	3710	97.632
2	2700	2750	-1600	450	450	3700	77.895
3	0	6400	-2500	1000	1000	3600	61.017
4	6500	-1900	0	-250	-250	4050	98.780
5	2500	2400	-1200	450	450	3500	76.087
6	0	6500	-2500	900	900	3100	53.448
FS Method							
1	6200	-1950	0	-240	-240	3720	98.674
2	2600	2700	-1500	460	460	3700	78.390
3	0	11000	-7000	1000	1000	3700	61.667
4	6460	-1920	0	-240	-240	4055	99.877
5	2400	2300	-1000	450	450	3420	74.348
6	0	4600	-1400	930	930	3300	65.217

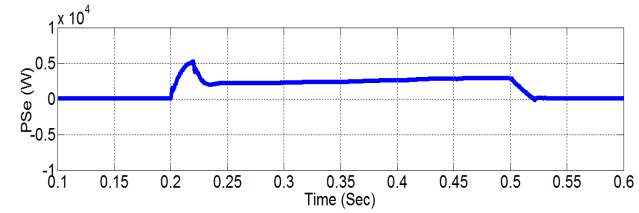

(a) 2UPQC

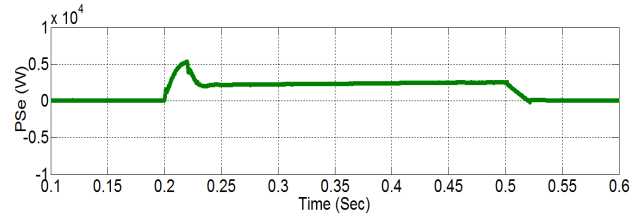

(b) 2UPQC-1PV

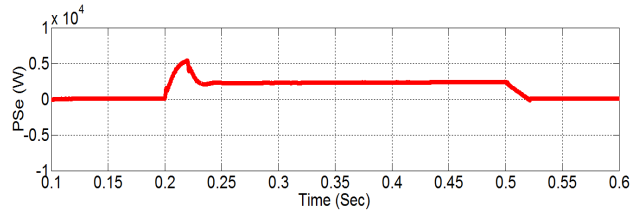

(c) 2UPQC-2PV

Figure 21. The performance of P_{Se} using the FS method on OM 5 (D-Sag-NLL)

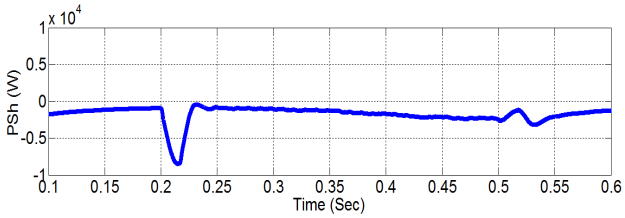

(a) 2UPQC

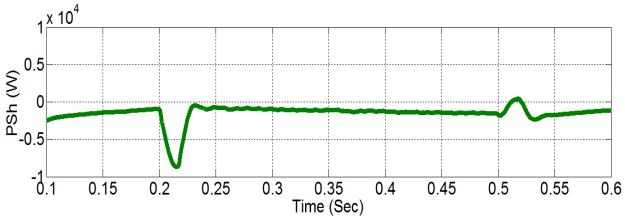

(b) 2UPQC-1PV

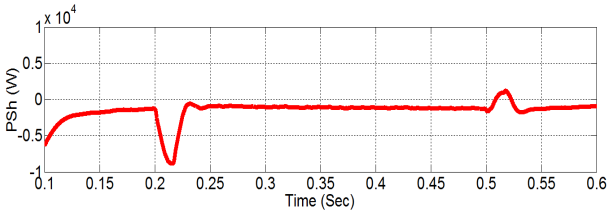

(c) 2UPQC-2PV

Figure 22. The performance of P_{Sh} using the FS method on OM 5 (D-Sag-NLL)

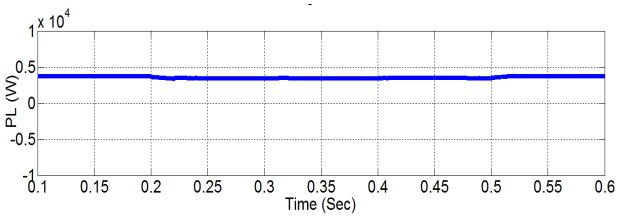

(a) 2UPQC

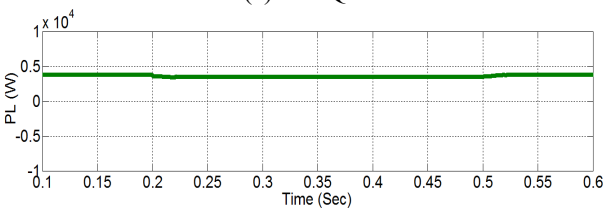

(b) 2UPQC-1PV

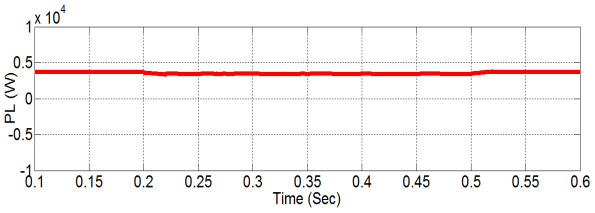

(c) 2UPQC-2PV

Figure 23. The performance of P_L using the FS method on OM 5 (D-Sag-NLL)

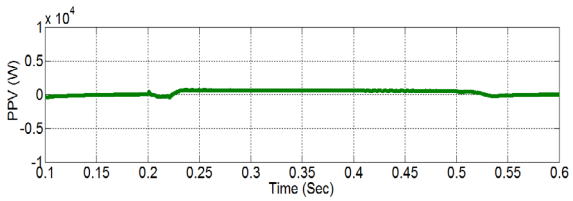

(a) 2UPQC-1PV

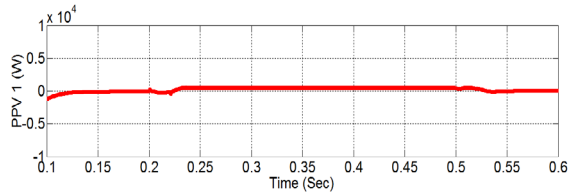

(b) 2UPQC-2PV

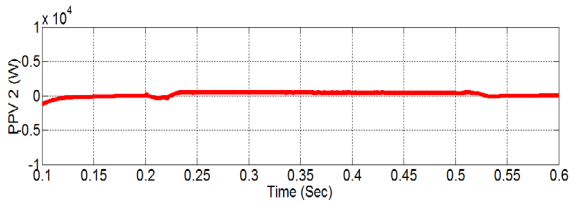

(c) 2UPQC-2PV

Figure 24. The performance of P_V using the FS method on OM 5 (D-Sag-NLL)

Figure. 25 to Figure. 29 presents the performance of: P_S, P_{Se}, P_{Sh}, P_L, and P_{PV} for the configuration of: (a) 2UPQC, (b) 2UPQC-1PV, and (c) 2UPQC-2PV respectively, using the FS method on OM 6 (D-Inter-NLL).

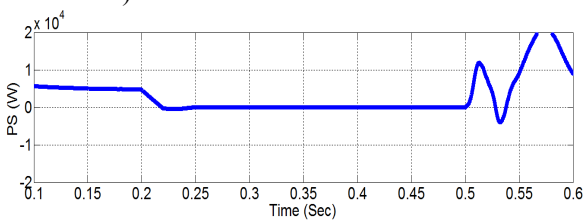

(a) 2UPQC

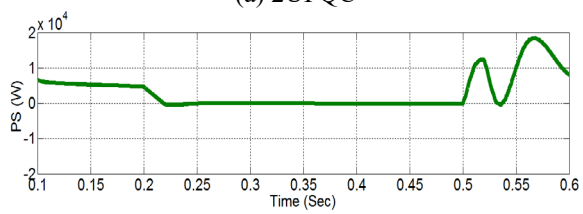

(b) 2UPQC-1PV

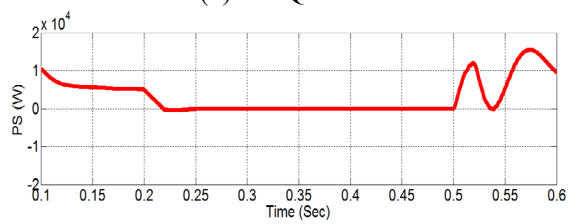

(c) 2UPQC-2PV

Figure 25. The performance of P_S using the FS method on OM 6 (D-Inter-NLL)

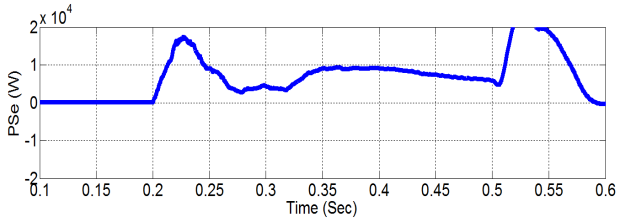

(a) 2UPQC

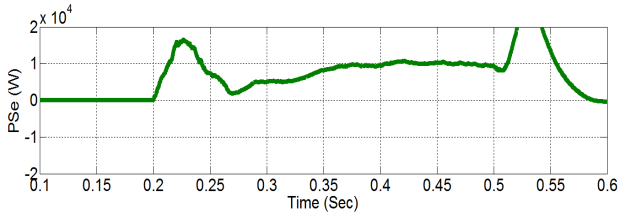

(b) 2UPQC-1PV

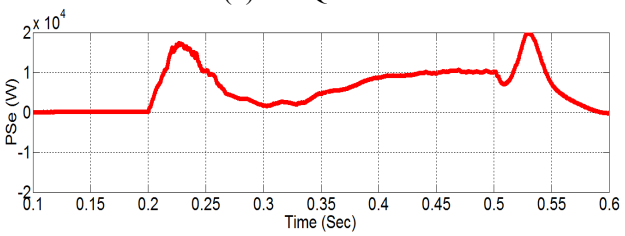

(c) 2UPQC-2PV

Figure 26. The performance of P_{Se} using the FS method on OM 5 (D-Sag-NLL)

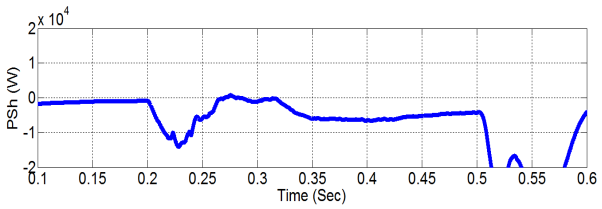

(a) 2UPQC

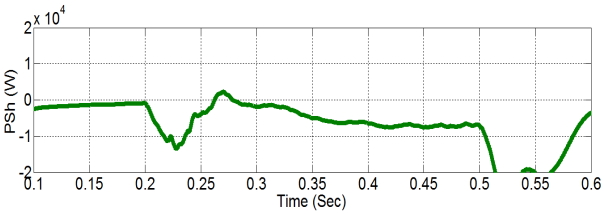

(b) 2UPQC-1PV

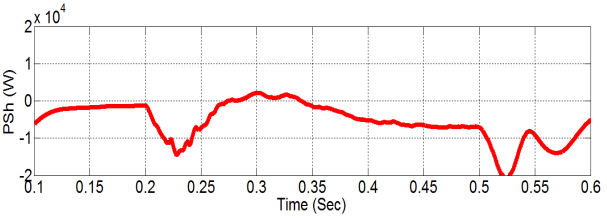

(c) 2UPQC-2PV

Figure 27. The performance of P_{Sh} using the FS method on OM 6 (D-Inter-NLL)

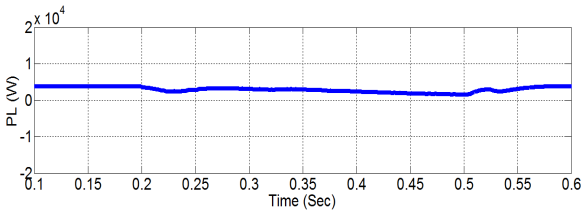

(a) 2UPQC

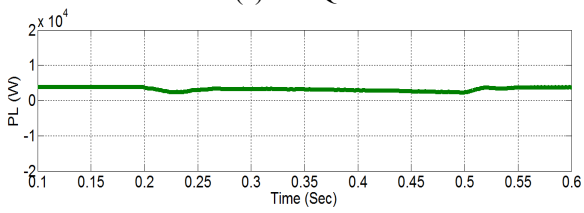

(b) 2UPQC-1PV

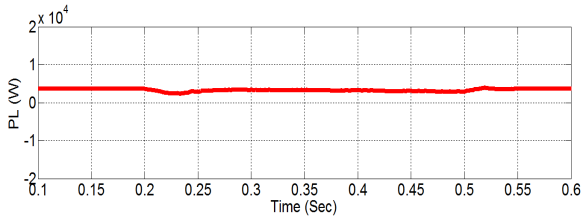

(c) 2UPQC-2PV

Figure 28. The performance of P_L using the FS method on OM 6 (D-Inter-NLL)

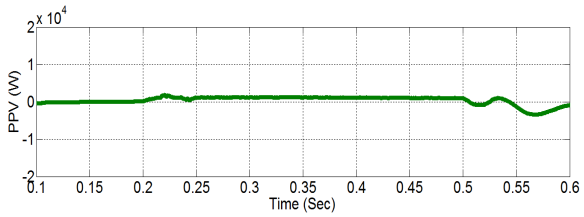

(a) 2UPQC

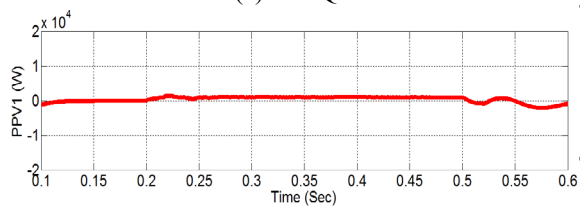

(b) 2UPQC-1PV

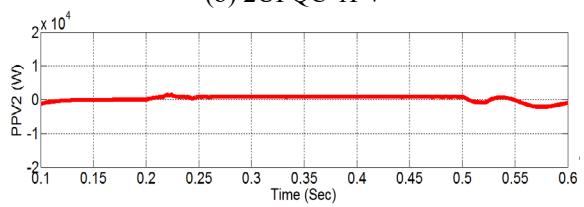

(c) 2UPQC-2PV

Figure 29. The performance of P_V using the FS method on OM 6 (D-Inter-NLL)

Figure. 20.a to Figure. 23.a presents the 3P3W system performance when experiencing OM 5 disturbances at t = 0.2 seconds to t = 0.5 sec and is resolved by the 2UPQC configuration using

the FS method. In this configuration the source real power (P_S) decreases to 2500 W (Figure. 20.a), the series real power (P_{Se}) increases by 2370 W (Figure. 21.a), and the shunt real power (P_{Sh}) decreases by -1300 W (Figure. 22.a), so the load real power (P_L) becomes 3425 W (Figure.23.a). Figure.20.b to Figure.24.a presents the 3P3W system performance when experiencing OM 5 disturbances at t = 0.2 sec to t = 0.5 sec and is resolved by the 2UPQC-1PV configuration using the FS method. In this configuration the source real power (P_S) decreases to 2400 W (Figure. 20.b), the series real power (P_{Se}) (Figure. 21.b) increases by 2370 W, and the shunt real power (P_{Sh}) decreases by -1300 W (Figure. 22.b), and PV1 injects the power (P_{PV1}) of 560 W (Figure.24.a) so that the load real power (P_L) becomes 3430 W (Figure. 23.b). Figure.20.c to Figure. 24.b and Figure 24.c presents the 3P3W system performance when experiencing OM 5 disturbances at t = 0.2 sec to t = 0.5 sec and is resolved by the 2UPQC-2PV configuration using the FS method. In this configuration, the source real power (P_S) decreases to 2400 W (Figure. 20.c), the series real power (P_{Se}) increases by 2300 W (21.c), and the real shunt power (P_{Sh}) decreases by -1000 W (Figure. 22.c), and PV1 and PV2 inject the power (P_{PV1} and P_{PV2}) of 450 W and 450 W respectively (Figure. 24.b and Figure. 24.c), so the load real power (P_L) to 3420 W (Figure.23.c).

Figure. 25.a to Figure. 29.a presents the 3P3W system performance when experiencing OM 6 disturbances at t = 0.2 sec to t = 0.5 sec and is resolved by the 2UPQC configuration using the FS method. In this condition the source real power (P_S) decreases to 0 W (Figure. 25.a), the series real power (P_{Sh}) increases by 9000 W (Figure. 26.a), and the shunt real power (P_{Se}) decreases by-6000 W (Figure.27.a), so the load real power (P_L) drops by 2900 W (Figure. 28.a). Figure. 25.b to Figure. 29.a presents the 3P3W system performance when experiencing OM 6 disturbances at t = 0.2 sec to t = 0.5 sec and is resolved by the 2UPQC-1PV configuration using the FS method. In this configuration, the source real power (P_S) drops to 0 W (Figure. 25.b), the series load power (P_{Se}) increases by 8000 W (Figure. 26.b), and the shunt real power (P_{Sh}) decreases by -5000 W (Figure. 27.b), and PV1 helps inject the power (P_{PV1}) of 1100 W (Figure. 29.a) so that the load real power (PL) increases slightly to 3150 W (Figure. 28.b). Figure. 25.c to Figure.29.b and Figure.29.c presents the 3P3W system performance when experiencing OM 6 disturbances at t = 0.2 sec to t = 0.5 sec and is resolved by the 2UPQC-2PV configuration using the FS method. In this configuration, the source real power (P_S) drops to 0 W (Figure. 25.c), the series real power (P_{Se}) increases by 4600 W (Figure. 26.c), and the shunt real power (P_{Sh}) decreases by -1400 W (Figure. 27.c), and PV1 and PV2 help inject the power (P_{PV1} and P_{PV2}) of 930 W and 930 W respectively (Figure. 29.b and Figure. 29.c) so that the load real power (P_L) increases to 3300 W (Figure 28.c).

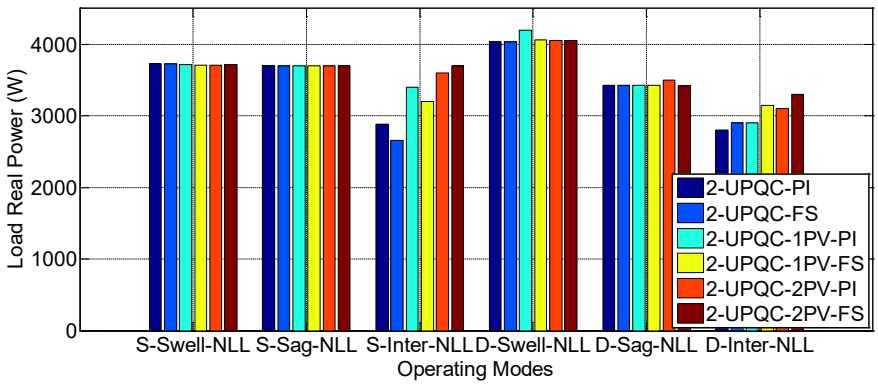

Figure 30. Performance of load real power

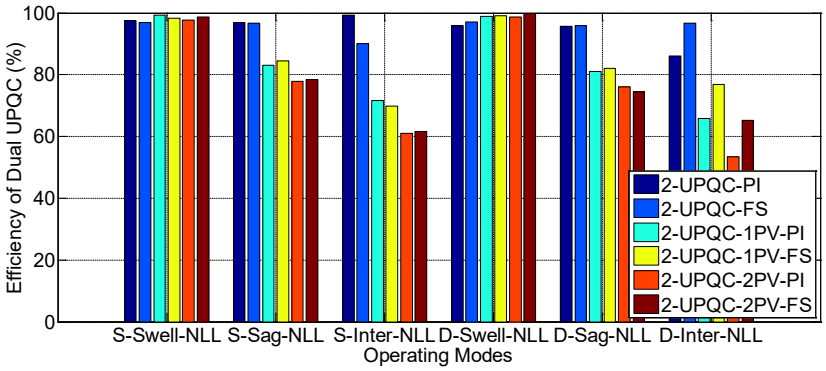

Figure 31. Performance of dual-UPQC efficiency

Figure. 30 presents that in the 2UPQC, 2UPQC-1PV, and 2UPQC-2PV configurations using the PI and FS methods, the OM 4 disturbance is able to produce higher real load power (P_L above 4030 W) than the OM 1 interference (P_L above 3712 W). This condition presents that the distortion of the source voltage in the Swell-NL distorted causes an increase in the load real power compared to the undistorted source voltage. In the same three configurations and using the PI and FS methods, the OM 5 disturbance produces lower load real power (P_L above 3420 W) than the OM 2 disturbance (P_L above 3700 W). This condition shows that the distorted source voltage in the Sag-NL disturbance causes a decrease in the load real power compared to the undistorted source voltage. In the same three configurations and using the PI and FS methods, the OM 3 disturbance is able to produce load real power higher than the OM 6 disturbance of 3600 W and 3700 W, compared to the 2UPQC and 2UPQC-1PV configurations. In the OM 6 disturbance, the 2UPQC-2PV configuration with PI and FS control is also capable of producing a higher load real power of 3100 W and 3300 W respectively than the 2UPQC and 2UPQC-1PV configurations. In OM 3 and OM 6, the FS method is able to produce higher real load power of 3700 W and 3300 W, respectively, compared to the PI method of 3600 W and 3100 W.

Using (15), the efficiency of load real power on each OMs and dual-UPQC configurations is obtained and the results are presented in Figure. 31. It shows that in the 2UPQC, 2UPQC-1PV, and 2UPQC-2PV configurations using the PI and FS methods, the OM 4 disturbance is able to produce a slightly higher efficiency than the OM 1 disturbance. In the three same configurations and using the PI and FS methods, OM 5 disturbance produces lower system efficiency than OM 2 disturbance. In the same three configurations and using PI and FS methods, OM 6 disturbance results in lower system efficiency than OM 3 disturbance. In OM 3 disturbance, 2UPQC-2PV configurations with PI and FS control are able to produce The lowest system efficiency was 61,017% and 61,667%, respectively, compared to the 2UPQC and 2UPQC-1PV configurations. In OM 6 disturbance, the 2UPQC-2PV configuration with PI and FS control is also able to produce the lowest system efficiency of 53,448% and 65,217% respectively compared to the 2UPQC and 2UPQC-1PV configurations. This condition shows that increasing the integration of the number of PV arrays (PV 1 and PV 2) in the dual-UPQC circuit will increase system losses so that the 2UPQC-2PV configuration produces the smallest system efficiency compared to the 2UPQC and 2UPQC-1PV configurations. In OM 3 and OM 6, the FS method is able to produce a higher efficiency of 61,667% and 65,217% respectively, compared to the PI method of 53,448% and 61,017%, respectively.

4. Conclusion

The 2UPQC-2PV to configuration to enhance load real power flow performance in a 380 V (L-L) with a frequency of 50 Hz on 3P3W has been implemented and validated with the 2UPQC and 2UPQC-1PV configurations. The simulation of disturbance in each model configuration consists of six OMs. The Dual-FS method is used to overcome the weaknesses of the Dual-PI control in determining the optimum parameters of proportional and integral constants. In OM 3

and OM 6, the 2UPQC-2PV configuration with Dual-PI and Dual-FS controls is able to maintain a higher load voltage than the 2UPQC and 2UPQC-1PV configurations. In OM 3 and OM 6, the 2UPQC-2PV configuration with Dual-PI and Dual-FS controls is capable of producing higher real load power, compared to the 2UPQC and 2UPQC-1PV configurations. In OM 6, the 2UPQC configuration with the dual PI and dual FS methods is able to produce the lowest average THD of load voltage compared to the 2UPQC-1PV and 2UPQC-2PV configurations. In OM 3 and OM 6, the 2UPQC-2PV configuration with the Dual-FS method is able to produce higher load real power, compared to the Dual-PI method. Furthermore, in OM 3 and OM 6, the 2UPQC-2PV configuration with the Dual-FS method is also able to produce higher dual-UPQC efficiency, compared to the Dual-PI method. In the case of interruption voltage disturbances with sinusoidal and distorted sources, the 2UPQC-2PV configuration with dual-FS control can enhance load real power performance and dual-UPQC efficiency better than dual-PI control. The average load voltage of 2UPQC, 2UPQC-1PV, and 2UPQC-2PV configuration using dual FS is below the dual PI method, especially during OM 3 and OM 6. The percentage of average load voltage disturbance at OM 3 and OM 6 using the dual PI and dual FS methods is still greater than 5%. The use of PV arrays with higher power and advanced control base on artificial intelligence such as a combination of fuzzy logic control and artificial neural networks (ANFIS), can be proposed as future work to solve this problem.

5. Acknowledgments

The authors would like to thank DRPM, Deputy for Strengthening Research and Development, Kemenristek/BRIN Republic of Indonesia for financing this research. This paper was the outputs of Fundamental Research 2nd year and implemented based on the Decree Letter Number: B/87/E3/RA.00/2020 on 28 January 2020 and Second Amendment Contract Number: 008/SP2H/AMD/LT/MULTI/L7/2020 on 17 March 2020, and Second Amendment Contract Number: 048/VI/AMD/LPPM/2020/UBHARA on 11 June 2020.

6. References

[1]. B. Han, B. Hae, H. Kim, and S.Back, "Combined Operation of UPQC with Distributed Generation", *IEEE Transactions on Power Delivery*, Vol. 21, No. 1, pp. 330-338, 2006.

[2]. B.W. Franca and M. Aredes, “Comparisons between The UPQC and Its Dual Topology (iUPQC) in Dynamic Response and Steady-State”, *IECON-2011-37th Annual Conference of the IEEE Industrial Electronics Society*, Melbourne, VIC, Australia, 7-10 Nov. 2011.

[3]. V. Khadkikar, "Enhancing Electric PQ UPQC: A. Comprehensive Overview", *IEEE Transactions on Power Electronics*, Vol. 27, No. 5, pp. 2284-2297, 2012.

[4]. R. Panigrahi and R.K. Patjoshi, “Robust Extended Complex Kalman Filter Based LQR Control Strategy of Shunt Active Power Filter”, *International Journal on Electrical Engineering and Informatics*, Vol. 12, No. 2, pp. 278-295, June 2020.

[5]. P. Kumar, “Comparative Power Quality analysis of Conventional and Modified DSTATCOM Topology”, *International Journal on Electrical Engineering and Informatics*, Vol. 9, No. 4, pp. 786-799, December 2017.

[6]. M. Farhadi-Kangarlu, M.B. Torshakaan, and Y. Neyshabouri, “A Transformerless DSTATCOM Based on Cross-Switched Multilevel Inverter for Grid Voltage Regulation”, *International Journal on Electrical Engineering and Informatics*, Vol. 12, No. 3, pp. 398-417, September 2020.

[7]. Jayasankar V N and Vinatha U, Modified Instantaneous Power Theory and Fuzzy Logic Based Controller for Grid-connected Hybrid Renewable Energy System with Shunt Active Power Filter Functionality, *International Journal on Electrical Engineering and Informatics*, Vol. 11, No. 2, pp. 373-388, June 2019.

[8]. S.P. Singh, A.H. Bhat, and A. Firdous, “A Novel Reduced-Rule Fuzzy Logic Based Self-Supported Dynamic Voltage Restorer for Mitigating Diverse Power Quality Problems”, *International Journal on Electrical Engineering and Informatics*, Vol. 11, No. 1, pp. 51-79, March 2019.

[9]. Ahmed M. A. Haidar, C. Benachaibab, N. Julaia, and M.F. Abdul Malek, "Parameters Extraction of Unified Power Quality Conditioner on the Calculation of a Membership Function", *International Journal on Electrical Engineering and Informatics*, Vol. 9, No. 2, pp. 244-258, June 2017.
[10]. V. F. Pires, D. Foito, A. Cordeiro and J. F. Martins, "PV Generators Combined with UPQC Based on a Dual Converter Structure", *IEEE 26th International Symposium on Industrial Electronics (ISIE), Edinburgh-UK*, 19-21 June 2017.
[11]. R.J.M. dos Santos, J.C. da Cunha, and M. Mezaroba, "A Simplified Control Technique for a Dual Unified PQ Conditioner, *IEEE Transactions on Industrial Electronics*, Vol. 61, No. 11, Nopember 2014, pp. 5851-5860.
[12]. B.W. Franca, L.F. da Silva, and M. Aredes, "Comparison between Alpha-Beta and DQ-PI Controller Applied to IUPQC Operation", XI Brazilian Power Electronics Conference, Praiamar, Brazil 11-15 September 2011.
[13]. B.W. Franca, L.F. da Silva, and M.A. Aredes, "An Improved iUPQC Controller to Provide Additional Grid-Voltage Regulation as a STATCOM", *IEEE Transactions on Industrial Electronics*, Volume: 62, Issue: 3, 2015, pp. 1-8.
[14]. S.A. Oliveira da Silva, L.B.G. Campanhol, G.M. Pelz, and V. de Souza "Comparative Performance Analysis Involving a Three-Phase UPQC Operating with Conventional and Dual/Inverted Power-Line Conditioning Strategies", *IEEE Transactions on Power Electronics*, Volume: 35, Issue: 11, 2020.
[15]. N.S. Borse and S.M. Shembekar, "PQ Improvement using Dual Topology of UPQC", International Conference on Global Trends in Signal Processing, *Information Computing and Communication (ICGTSPICC)*, Jalgaon, India, 22-24 Dec. 2016, pp. 428-431.
[16]. R.A. Modesto and S.A. Oliveira da Silva, "Versatile Unified PQ Conditioner Applied to Three-Phase Four-Wire Distribution Systems Using a Dual Control Strategy", *IEEE Transactions on Power Electronics*, Volume: 31, Issue: 8, 2016, pp. 1-12.
[17]. R.A. Modesto, S.A. Oliveira da Silva, A.A. de Oliveira Júnior, "PQ Improvement using a Dual Unified PQ Conditioner/Uninterruptible Power Supply in Three-Phase Four-Wire Systems" *IET Power Electronics*, Volume: 8, Issue: 9, 2015, pp. 1595-1605.
[18]. S.M. Fagundes and M. Mezaroba, "Reactive Power Flow Control of a Dual Unified PQ Conditioner", *IECON 2016 - 42nd Annual Conference of the IEEE Industrial Electronics Society*, Florence, Italy, 23-26 Oct. 2016, pp. 1156-1161.
[19]. L.B.G. Campanhol, S.A.O. da Silva, and AA. de Oliveira Júnior, V.D. Bacon, "Single-Stage Three-Phase Grid-Tied PV System with Universal Filtering Capability Applied to DG Systems and AC Microgrids", *IEEE Transactions on Power Electronics*, Volume: 32, Issue: 12 , Dec. 2017, pp. 9131 - 9142.
[20]. A. Andrews and R. Scaria, "Three-Phase Single Stage Solar PV Integrated UPQC", 2019 *2nd International Conference on Intelligent Computing, Instrumentation and Control Technologies (ICICICT)*, 5-6 July 2019, Kannur, Kerala, India, pp. 1130-1134.
[21]. S.C. Ghosh and S.B. Karanki, "PV Supported Unified Power Quality Conditioner Using Space Vector Pulse Width Modulation" *2017 National Power Electronics Conference (NPEC)*, 18-20 Dec. 2017, Pune, India, pp. 264-269.
[22]. S. Devassy and B. Singh, "Design and Performance Analysis of Three-Phase Solar PV Integrated UPQC", *IEEE Transactions on Industry Applications*, Volume: 54, Issue: 1, Jan.-Feb. 2018, pp. 73 – 81.
[23]. L.B.G. Campanhol, S.A.O. da Silva, and AA. de Oliveira Júnior, V.D. Bacon, "Power Flow and Stability Analyses of a Multifunctional Distributed Generation System Integrating a Photovoltaic System with Unified Power Quality Conditioner", *IEEE Transactions on Power Electronics*, Volume: 34, Issue: 7, July 2019, pp. 6241-6256.
[24]. Amirullah, A. Soeprijanto, Adiananda, and O. Penangsang, "Power Transfer Analysis Using UPQC-PV System Under Sag and Interruption with Variable Irradiance", 2020 *International Conference on Smart Technology and Applications (ICoSTA)*, Surabaya, Indonesia, 20-20 Feb. 2020.

[25]. L.B.G. Campanhol, S.A.O. da Silva, and A.O. Azauri, “A Three-Phase Four-Wire Grid-Connected Photovoltaic System using a Dual Unified Power Quality Conditioner”, 2015 *IEEE 13th Brazilian Power Electronics Conference and 1st Southern Power Electronics Conference (COBEP/SPEC)*, 29 Nov.-2 Dec. 2015, Fortaleza, Brazil.
[26]. A.A. Al-Shamma'a and K.E. Addoweesh, “Dual Unified Power Quality Conditioner Based on Open-Winding Transformers and Series Converters for Grid-Connected PV Systems” *2017 9th IEEE-GCC Conference and Exhibition (GCCCE)*, 8-11 May 2017, Manama, Bahrain.
[27]. A. Amirullah, A. Adiananda, O. Penangsang, A. Soeprijanto, Load Active Power Transfer Enhancement Using UPQC-PV-BES System with Fuzzy Logic Controller, *International Journal of Intelligent Engineering and Systems*, Vol.13, No.2, 2020, pp. 330-349.
[28]. Y. Bouzelata, E. Kurt, R. Chenni, and N. Altin, "Design and Simulation of UPQC Fed by Solar Energy", *International Journal of Hydrogen Energy*, Vol. 40, 2015, pp. 15267-15277.
[29]. S.Y. Kamble and M.M. Waware, "UPQC for PQ Improvement", *Proceeding of International Multi Conference on Automation Computer, Communication, Control, and Computer Sensing (iMac4s)*, Kottayam, India, 2013, pp. 432-437.
[30]. M. Hembram and A.K. Tudu, “Mitigation of PQ Problems Using UPQC, *Proceding of Third International Conference on Computer, Communication, Control, and Information Technology (C3IT)*, 2015, Hooghly, India, 2015, pp.1-5.
[31]. Y. Pal, A. Swarup, and B. Singh, "A Comparative Analysis of Different Magnetic Support Three Phase Four Wire UPQCs-A Simulation Study", *Electrical Power and Energy System*, Vol. 47., 2013, pp. 437-447.
[32]. A. Kiswantono, E. Prasetyo, A. Amirullah, Comparative Performance of Mitigation Voltage Sag/Swell and Harmonics Using DVR-BES-PV System with MPPT-Fuzzy Mamdani/MPPT-Fuzzy Sugeno, *International Journal of Intelligent Engineering and Systems*, Vol.12, No.2, 2019, pp. 222-235.
[33]. 1159-1995 Standards-IEEE Recommended Practice for Monitoring Electric PQ, 29.240.01-Power Trans. and Distribution Networks in General, 30 Nov 1995, pp. 1-70.
[34]. M. Ucar and S. Ozdemir, “3-Phase 4-Leg Unified Series–Parallel Active Filter System with Ultracapacitor Energy Storage for Unbalanced Voltage Sag Mitigation”, *Electrical Power and Energy Systems*, Vol. 49, pp. 149-159, 2013.

Amirullah was born in Sampang East Java Indonesia, in 1977. He received B.Eng and M.Eng degrees in electrical engineering from the University of Brawijaya Malang and ITS Surabaya, in 2000 and 2008, respectively. Since 2002, He also has worked as a lecturer in Universitas Bhayangkara Surabaya. He obtained a Doctoral degree from electrical engineering ITS Surabaya in 2019 from Power System and Simulation Laboratory (PSSL). He has 13 publications in Scopus with h-index 5. His research interest includes power distribution modelling and simulation, power quality, harmonics mitigation, design of filter/power factor correction, and renewable energy base on artificial intelligence. He also has been an IEEE member since 2019.

Adiananda was born in Nganjuk East Java Indonesia, in 1973. He received bachelor degree in electrical engineering from Universitas Bhayangkara Surabaya and a master of computer science from Gadjah Mada University (UGM) Yogyakarta, in 1996 and 2016, respectively. Since 1998, He has worked as a lecturer in Universitas Bhayangkara Surabaya. He is interested in the research of the application of artificial intelligence in modelling power electronics and computer systems.

Ontoseno Penangsang was born in Madiun East Java Indonesia, in 1949. He received a bachelor in electrical engineering from ITS Surabaya, in 1974. He received and M.Sc. and Ph.D. degree in Power System Analysis from the University of Wisconsin, Madison, USA, in 1979 and 1983, respectively. He is currently a professor at the Department of Electrical Engineering and ITS Surabaya. He has a long experience and main interest in power system analysis (with renewable energy sources), design of power distribution, power quality, and harmonic mitigation in industry. Professor Ontoseno Penangsang has 77 publications in Scopus with h-index 9.

Adi Soeprijanto was born in Lumajang East Java Indonesia, in 1964. He received a bachelor in electrical engineering from ITB Bandung, in 1988. He received a master of electrical engineering in control automatic from ITB Bandung. He continued his study to Doctoral Program in Power System Control at Hiroshima University Japan and was finished it's in 2001. He is currently a professor at the Department of Electrical Engineering and a member of PSSL in ITS Surabaya. His main interest includes power system analysis, power system stability control, and power system dynamic stability. He had already achieved a patent in the optimum operation of the power system. Professor Adi Soeprijanto has 144 publications in Scopus with h-index 12.